DIPLOMARBEIT

Comparison of the dosimetric impact of 125-I and 106-Ru plaque brachytherapy of uveal melanoma using a novel treatment planning software

zur Erlangung des akademischen Grades

Diplom-Ingenieurin

im Rahmen des Studiums

Biomedical Engineering

an der Technischen Universität Wien

eingereicht von

Patricia Braun, BSc

Matrikelnummer 01325687

ausgeführt am Atominstitut

der Fakultät für Physik der Technischen Universität Wien

in Zusammenarbeit mit der Universitätsklinik für Strahlentherapie der Medizinischen Universität Wien und dem Austrian Institute of Technology

Betreuung

Betreuer: Univ.-Prof.DI.Dr. Dietmar Georg

Mitwirkung: Gerd Heilemann, PhD und Dr. Matthias Blaickner

Wien, 12.12.2018

_____	_____
Unterschrift Studentin	Unterschrift Betreuer

Acknowledgements

First of all, I specially want to thank Gerd Heilmann, PhD and Dr. Matthias Blaickner who both supervised me during my Master thesis. Both of them helped me a lot with theoretical and practical issues and I am very thankful for their invested time. I would also like to thank Prof. Dietmar Georg who supported me during this time and Dr. Roman Dunavölgyi who answered all the medical questions. Thanks as well to Ass.-Prof.in Nicole Nesvacil who gave me a lot of background information. Many thanks also to Lukas Fetty, MSc. who invested a lot of time helping me with some issues concerning the 3D animation software Houdini FX.

Statutory declaration

I declare that I composed this thesis solely by myself, that the work contained herein is my own, that I have not used other sources than stated, and that I have cited all the materials that have either been used verbatim or by contend from the used source.

Vienna, December 2018 _____

Signature

Zusammenfassung

Aderhautmelanome sind die am häufigsten auftretenden Augentumore weltweit. Zu einer der bevorzugten Behandlungsmethoden dieser, zählt heutzutage die Brachytherapy. Dabei werden vorwiegend ^{106}Ru oder ^{125}I COMS Augenapplikatoren verwendet.

In den letzten Jahren ist an der Universitätsklinik für Strahlentherapie der Medizinischen Universität Wien (MUW), ein wissenschaftliches Behandlungsplanungssystem für die Therapie mit Ruthenium-106 Augenapplikatoren entwickelt worden. Es ermöglicht die Simulation der Behandlung unterschiedlicher Tumorgrößen und Tumorpositionen und die Untersuchung der daraus resultierenden dosimetrischen Auswirkung auf die Risikoorgane. Ziel dieser Masterarbeit ist es, dieses Behandlungssystem durch die Einbindung eines Iod-125 COMS (Collaborative Ocular Melanoma Study) Augenapplikators zu erweitern. Zusätzlich zu den Dosis–Nachschlagtabellen, welche mittels Monte Carlo Simulationen generiert und anschließend in die 3D Animationssoftware Houdini Apprentice Non-Commercial 16.0.633 (Side Effects Software Inc., Toronto, Canada) implementiert wurden, wurde ein geometrisches Model des ^{125}I COMS Augenapplikators entworfen. Dieser Schritt soll einen dosimetrischen Vergleich beider Modalitäten, den ^{125}I COMS und ^{106}Ru Augenapplikatoren, ermöglichen, um in weiterer Folge eine Empfehlung für die möglichst optimale Applikatorauswahl und Therapieplanung zu erarbeiten.

Um individuelle Krankheitsbilder entsprechend des Behandlungsplanes und des Beladungsdiagrammes des Augenapplikators simulieren zu können, wurden die einzelnen Dosis–Nachschlagtabellen, welche jeweils ein Seed des ^{125}I COMS Augenapplikators repräsentieren, einzeln implementieret. Dies ermöglicht die Simulation individueller Applikatorbelegungen. Mit Hilfe des neu generierten geometrischen Models des ^{125}I COMS Augenapplikators wurde die Tumor-Abdeckung für unterschiedliche Tumorgrößen und zwei unterschiedliche ^{125}I COMS Applikatorkonfigurationen untersucht. Diese ergab, dass der größte Tumor, welcher durch einen vollbelegten Augenapplikator noch vollständig abgedeckt werden kann, eine Höhe von 8 mm und einen maximalen Basisdurchmesser von 16 mm hat. Für einen Augenapplikator dessen äußerster Ring nicht mit Seeds belegt ist, reduziert sich der maximal abdeckbare Basisdurchmesser auf 14 mm für eine Höhe von 8 mm. Zusätzlich brachte die Studie hervor, dass die Tumor-Abdeckung, verglichen zu jener der CCA und CCB ^{106}Ru Augenapplikatoren Studie, durchgeführt von Fetty [1], stabiler im Hinblick auf Applikator-Verschiebungen ist.

Neben der Tumor-Abdeckung wurden auch die absorbierten Dosiswerte der einzelnen Risikoorgane ausgewertet und mit den Resultaten in der vorangegangen Publikation [2] verglichen. Die Studie, welche im Zuge dieser Masterarbeit durchgeführt wurde, ergab, dass mit Hilfe der ^{125}I COMS Augenapplikatoren bessere Ergebnisse im Hinblick auf die Schonung der Retina erzielt werden können. Des Weiteren wurde festgestellt, dass der ^{125}I COMS Applikator bei der Behandlung eines posterior gelegenen Tumor näher am Sehnerv platziert werden kann und dieser zusätzlich weniger Dosis absorbiert.

Abstract

Uveal melanoma is the most common malignant intraocular tumor worldwide. These days one of the preferred treatment methods is brachytherapy, either using ruthenium-106 or iodine-125 COMS eye plaques.

At the Department of Radiation Oncology of the Medical University of Vienna a scientific version of a treatment planning system for uveal melanoma was developed in previous work using ^{106}Ru eye applicators. It enables to simulate the treatment of different tumor geometries and locations inside the eye and thereby to evaluate the dosimetrical impact on the organs at risk The purpose of this master thesis was to extend this in house developed software by including a model of the ^{125}I COMS (Collaborative Ocular Melanoma Study) plaque. Additionally, to the integration of existing dose lookup tables, generated with Monte Carlo simulations, into the 3D animation software Houdini Apprentice Non-Commercial 16.0.633 (Side Effects Software Inc., Toronto, Canada) a geometrical shape of the ^{125}I COMS plaque was implemented. Based on this a comparison of the dose distribution of the ^{106}Ru and the ^{125}I COMS plaque should be possible and thereby help to develop recommendations for the most optimal selection of the applicators and treatment planning.

In order to simulate individual symptoms according to the treatment plan and the loading diagram, the various dose lookup tables, each representing one seed of the ^{125}I COMS plaque were implemented individually. This step enables an individual occupancy of the plaque on demand. Using the newly implemented geometrical shape of the ^{125}I COMS plaque the tumor coverage for different tumor parameters and two different plaque configurations was investigated. It was found out that using a fully occupied plaque the largest coverable basal diameter of a tumor with 8 mm apex height is 16 mm. If a plaque configuration is applied were the outer ring of the seeds is spared the maximal basal diameter reduces to 14 mm for the same apex height. Additionally, it was found out that the coverage is more stable with regards to plaque displacements, comparing it to previous studies of the CCA and CCB ^{106}Ru plaque types by Fetty [1].

Furthermore, the absorbed dose of the organs at risk was investigated and compared to the ones observed by the previous study by Heilemann e*t al.* [2]. The study that was carried out in course of this master thesis showed that the ^{125}I COMS plaque is superior in sparing the retina. In addition, it was found out that treating a posterior located tumor the ^{125}I COMS plaque can be placed closer to the optic nerve and the optic nerve itself absorbed less dose.

Contents

List of Figures

List of Tables

List of Abbreviations

DNA	deoxyribonucleic acid
TCP	tumor control probability
NTCP	normal tissue control probability
OAR	organ at risk
SOBP	spread out Bragg peak
LINAC	Linear Accelerator
SRS	single fraction stereotactic radiosurgery
SRT	fractionated stereotactic radiotherapy
COMS	Collaborative Ocular Melanoma Study
^{106}Ru	ruthenium-106
^{125}I	iodine-125
^{106}Rh	rhodium-106
^{109}Pd	palladium-109
^{124}Xe	xenon-124
MC	Monte Carlo
TG	Task Group

1. Introduction

1.1. Radiotherapy

1.1.1. General concept of Radiotherapy

Depending on the type of the tumor and its stage radiotherapy is a treatment method that can either be used palliative, curative or after surgical intervention to prevent tumor recurrence. The most important factors regarding the effectiveness of this treatment method are the particle type, its energy, the irradiation time and the targeted volume. Radiotherapy bases on the damaging effect of ionizing radiation on malignant as well as healthy tissue cells.

Ionizing radiation has enough energy to remove bound electrons from an atom of the irradiated material whereas non-ionizing irradiation can only cause excitation, i.e. electrons are not removed but raised to a higher energy state.

In general, one can differentiate between directly and indirectly ionizing radiation. If the kinetic energy of charged particles such as protons or electrons is high enough these particles can produce direct ionization by collision. During this process they loose energy and at one point become non-ionizing, dissipating the remaining energy either by excitation or elastic scattering processes [3].

Indirectly ionizing radiation is based on uncharged particles such as photons or neutrons that firstly transfer their energy to charged ones which then ionize the material and cause biological damage [3].

There are two different ways chemical and biological damage can be induced by ionizing radiation. Either the electrons interact directly with the DNA or firstly interact with some other atoms or molecules within the cell, such as water, producing free radicals that can further interact with the DNA. These free radicals are not charged but do have an unpaired valence electron and hence are highly chemically reactive. They can induce some breakage of chemical bonds that can further lead to biological effects. The predominating radicals that are produced inside the human body by radiolysis of water are the hydroxyl radical (OH•) and the water ion (H_2O^+) [4], [5].

Biological damage that can occur due to ionizing radiation can be single-strand-breaks or double-strand-breaks of the DNA. In contrast to the double-strand-breaks the single-strand-breaks can be easily repaired by taking the opposite strand of the DNA double helix as a template. If the double-strand-breaks are not repaired in a correct way they can lead to deletions, translocations and fusion in the DNA, which can further result in genomic

rearrangements, such as chromosomal aberrations, mostly found within tumor cells. Chromosomal aberrations base on the incorrect coalescence of two broken DNA fragments. [4], [6].

Radiation induced damage can be divided into three classes. The irreversible lethal damage that leads to cell death. The sublethal damage that can be repaired in a few hours as long as no other sublethal damage is induced that would worsen the state of the cell ending in lethal damage. The third category is the potentially lethal damage. This one can be repaired by manipulation, if the cell stays in a non-dividing state of the cell cycle [5].

There are two different types of cell death that can occur after irradiation. Apoptosis, also called programed cell death, is a homeostatic mechanism which normally occurs during cell development. On the one hand side it helps to maintain the cell populations in the tissues but on the other hand side it is also used as a defense mechanism if cells are damaged. Before the damaged cells are proliferating, they die. Whereas necrosis is a toxic process and can't be controlled by the cell itself but is triggered by external factors. During an apoptosis the cell membrane remains functional, the cell shrinks and no inflammation process occurs. If a cell dies by necrosis it gets bigger by swelling, the cell membrane is disrupted and it normally ends with an inflammation [7].

1.1.2. Tumor Control Probability and Normal Tissue Complication Probability

The fact that the healthy tissue cells are less sensitive to radiation than malignant cells allows the preservation of normal tissue. This can be explained by reference of Figure 1. The tumor control probability (TCP) increases with the delivered dose. The higher the applied dose the more likely it is to destroy the targeted volume. On the other hand also the normal tissue complication probability (NTCP) increases since more normal tissue cells are damaged. In the treatment with radiotherapy the right balance between TCP and NTCP has to be achieved, by keeping the TCP to a maximum while keeping the NTCP to a minimum. In general, the therapeutic window, indicated by the area between both curves, has to be increased by shifting the TCP curve to the left while shifting the NTCP curve to the right. These can be achieved by many different factors such as radioprotectors that are applied to the healthy tissue to protect them from the radiation. [8], [9].

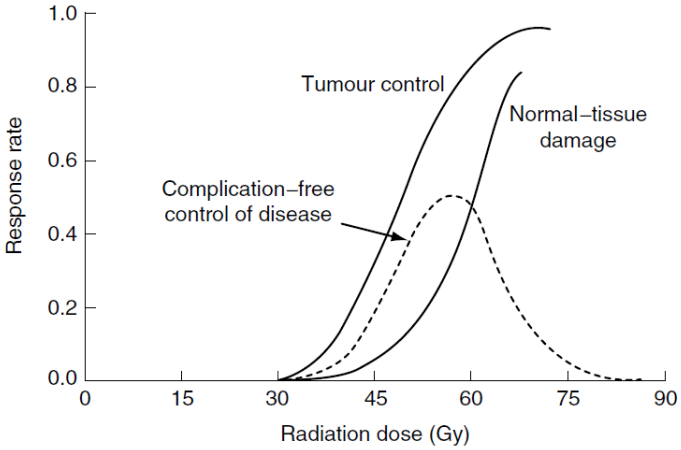

Figure 1: Illustration of the dose response curves of the tumor control and normal-tissue damage (solid lines). Out of these two curves the probability of the complication-free tumor control has been calculated and is depicted as the dashed line. (from [8]*)*

1.1.3. The volume effect

Besides the particle type, its energy and the irradiation time the severity of the damage to normal tissue cells caused by radiation mostly depends on the volume of the tissue being irradiated. This is called volume effect and there are some differences among organs, depending on their structural organization. They can be classified as serial or parallel organs. Serial organs are characterized by a tube-like structure where irradiation of a small segment of the organ results in a complete inactivation of the whole. Parallel organs can still function after a partial irradiation since they only get inactive if all the sub-volumes are damaged. On the right side of Figure 2 it can be seen that with regard to the same dose the probability of morbidity for a serial organ is higher than for a parallel one. A general example for serial ones is the spinal cord. The lung as well as the kidney are parallel ones. Ophthalmic structures that belong to the serial organs are the optic nerve, the lens and the macula. The retina would be an example for the parallel organs inside the eye. Besides serial and parallel organs there are also intermediate ones such as the brain, having both properties, serial as well as parallel ones [8], [10].

For serial organs the variation of the NTCP with volume at a constant dose is linear for small NTCPs. For parallel organs a threshold effect is observed, where below a critical volume the NTCP is quite small and above it the NTCP rises with increasing irradiated volume [11].

The healthy serial or parallel organs surrounding the tumorous tissue which can be damaged irreversibly by radiation and thereby have to be considered in the treatment planning to keep their morbidity rate as low as possible, are called organs at risk (OAR).

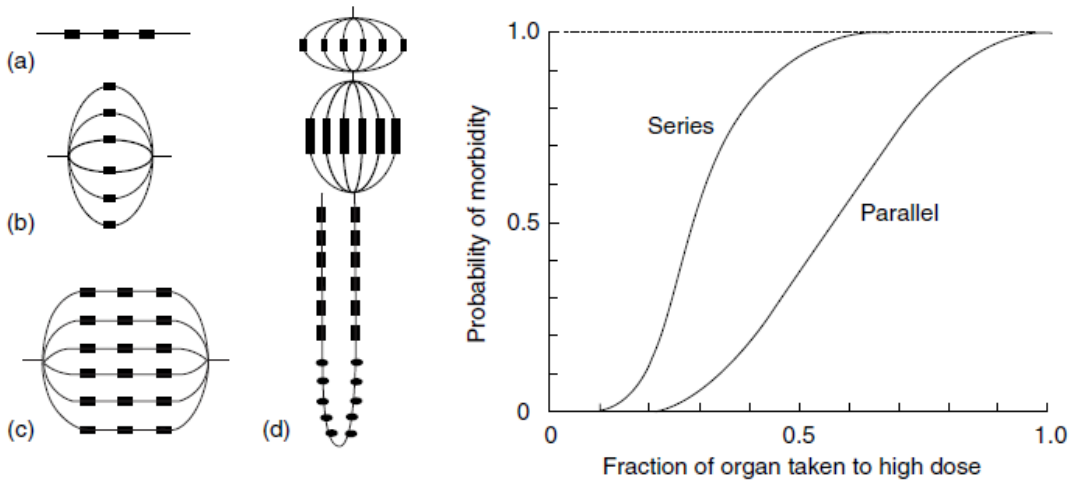

Figure 2: Schematic illustrations showing the concept of the (a) serial, (b) parallel and (c) serial-parallel organs. (d) is a combination of serial and parallel organs. On the right side, it can be seen that there is a difference in the relationship of the complication probability vs. partial high-dose volume between serial and parallel organs (from [8]*).*

1.2. Dose delivery techniques

1.2.1. External proton beam therapy

External proton therapy works due to the physical properties of accelerated protons which are slowed down in matter due to energy transfer. This phenomenon is described by the so called stopping power.

$$S(E) = -\frac{dE}{dx} \tag{1}$$

The stopping power indicates the loss of energy along a certain distance.

At a certain point the loss of energy reaches a maximum. This point is called Bragg peak. After the Bragg peak there is a steep decline of the dose. This process is quite advantageous compared to brachytherapy and stereotactic photon therapy. On the one side it leads to a delivery of a homogenous radiation dose to the entire tumor and on the other hand the healthy tissue surrounding the tumor is spared, especially the one behind the tumor, due to the sharp decrease in dose after the Bragg peak. Despite this it is important to keep the high entrance dose in mind [12].

The energy of the beam and hence the range of the protons, that are needed for the treatment are defined by the thickness of the target volume and its depth within the patient. In many cases one single peak is too narrow for clinical applications and therefore various

single peaks from different energy beams superimposed, resulting in a plateau called spread out Bragg peak (SOBP) and a homogeneously covered tumor. The modulation of the beam is achieved by using a wheel with changing thicknesses resulting in different absorption levels of the proton beam and subsequently in different depths [13].

Figure 3 shows both, a normal Bragg peak with only one single peak at the end of the targeted volume and one spread out Bragg peak whose plateau spans over the whole tumor.

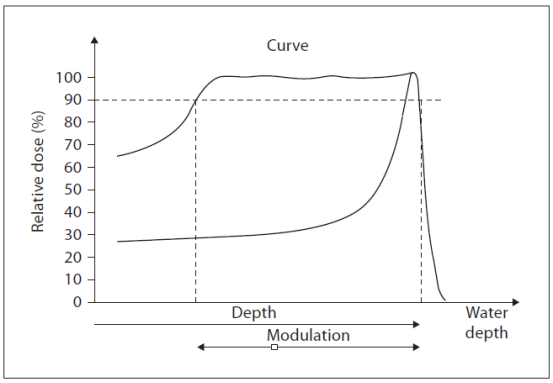

Figure 3: Typical depth dose distribution of a proton beam within water. On the one hand side the SOBP resulting in the homogenous dose delivery to the entire tumor and the sparing of the tissue behind the tumor can be seen. On the other hand the typical single Bragg peak can be seen after which the dose is falling off steeply, hence resulting in the sparing of the normal tissue behind the delivery point. (from [12]*).*

1.2.2. Stereotactic photon therapy

Stereotactic photon therapy is the most frequent external treatment modality and practiced in a lot of radiotherapy centers around the world. This treatment method is based on high energy electrons and photons produced in a Linear Accelerator (LINAC). Compared to charged particles photon can travel further until they get absorbed by the body, resulting in a flatter dose decrease. In general, two different methods can be distinguished. Single fraction stereotactic radiosurgery (SRS) uses only one single very large fraction trying to inactivate the growth potential of the cells within the volume of interest. On the contrary fractionated stereotactic radiotherapy (SRT) tries to preserve the normal tissue cells within the volume of interest as well as the ones in the surrounding tissue, by using not only one single fraction but multiple fractions [14]–[18].

1.2.3. Brachytherapy

Brachytherapy is a short distance treatment modality, locally irradiating the targeted volume. Therefore, small capsules containing a radioactive source, emitting either beta or gamma radiation, can be placed nearby or within the affected volume. This enables the

delivery of high doses exactly to the target of interest by sparing the surrounding healthy tissue.

For delivering the dose to the affected volume two different ways can be used. Either it can be delivered in a short period of time by removing the radioactive source after the treatment is finished (temporary implants) or the patient is treated as long as the radioactive source is decaying (permanent implant). Therefore, the radioactive source stays within the body and is not removed.

The modalities applied most often are the intracavitary method, where the sources are placed in cavities of the body close to the tumor and the interstitial method where the radioactive sources are placed directly inside the tumor volume. Techniques such as surface plaque, intraluminal, intraoperative and intravascular source applications are generally less applied [19].

1.3. Uveal melanoma

Uveal melanoma is one of the most frequent occurring malignant intraocular tumors. It arises from the uveal layer which includes the choroid, the ciliary body and the iris. Although the probability of its occurrence is 75% of all intraocular tumors it is rare with a mean incidence of less than one new case per 100.000 inhabitants a year. This results in a small fraction of 0.003% of all cancer incidences, predominating in the male population [20], [21].

People all over the world suffer from uveal melanomas but in comparing the different parts of the world different trends in the occurrence can be seen. While there hasn't been any change in the incidences in the U.S., Denmark or Finland over the last 30 years, Sweden records an annual relative decrease. The populations that are least likely to suffer from uveal melanomas and for whom a low incidence rate is reported are Africans and African-Americans, Asians as well as the American population of Asian descent. Within Europe an increasing gradient of incidences from south to north can be seen. By the time when uveal melanomas are diagnosed most of the patients are within their sixth decade of life having reached the age of 55 in most of the cases. Incidence rates of uveal melanoma show a similar behavior in the U.S. and Europe, with an increasing rate till the age of 70 and 75 years in the U.S. and Europe, respectively [22].

The lack of any symptoms in the early stage poses a challenge to the diagnosis of uveal melanomas. Only at an advanced stage loss and impairment of vision, a limited visual field and pain are reported. All these symptoms mostly depend on the extent and the location of the tumor within the eye [20].

In the early days when clinicians started to treat patients suffering from uveal melanomas, enucleation has been the preferred therapy. But with time Zimmermann *et al.* [12] have shown that this treatment method has been not efficient enough in preventing the spreading of metastasis, hence the start of radiotherapy in the 80ies. This new method was found to be a good alternative regarding tumor control probability (TCP) and preservation of vision. Nowadays, depending on the thickness, the diameter and the location of the tumor within the eye, different types of radiotherapy, such as proton radiotherapy, stereotactic photon therapy or eye plaque brachytherapy, can be used [12], [20]

1.4. Treatment techniques of ocular tumors

1.4.1. Enucleation

Enucleation is the surgical removal of the eye. Although this standard treatment method was replaced by radiotherapy in the 80ies, it is still sometimes used to treat uveal melanoma that are either confined to the eye or have a diameter bigger than 10 mm. Latter is done because it shows an improved local tumor control and the ocular morbidity is less than in other treatment procedures. In some cases photon-based external beam radiotherapy is used prior to enucleation and in others radiation therapy is used afterwards to make sure that there are no residuals left [20], [23].

1.4.2. Proton therapy

The first ones who started to use proton therapy for the treatment of uveal melanoma have been Gragoudas and his group [12] in Boston in 1975. Afterwards the usage of this method spread all around the world resulting in thousands of patients that have been treated in the last 30 years [12].

As mentioned earlier in section 1.2.1 if proton beams are used for treating patients the dose is homogenous delivered to the entire tumor but sparing the surrounding tissue. This fact is very important for treating uveal melanoma because this type of tumor is very radioresistant and thereby a high dose has to be applied to it [12].

The first step treating uveal melanoma using proton beams would be to localize the tumor by clip positioning which is done during a surgery, by suturing tantalum rings of 2.5 mm to the sclera surrounding the tumor base. Two weeks after the surgery the proton beam therapy can be started [12].

Usually only tumors with a maximum basal diameter of 20 mm or a thickness, that indicates the distance of the base to the apex, of 12 mm are treated with external proton beam therapy, otherwise the probability to preserve the vision and the globe is very low. If the tumor is

smaller in size the preferred treatment method would be brachytherapy using ^{106}Ru plaques or ^{125}I COMS (Collaborative Ocular Melanoma Study) plaques [12].

1.4.3. Stereotactic photon therapy

In the last couple of years stereotactic photon therapy was investigated for the treatment of uveal melanoma. The therapeutic single dose which is applied using single fraction stereotactic radiosurgery (SRS) was reduced to 35 Gy. This treatment method is either usually done with a gamma knife or a cyberknife. The second method that gained of interest for treating patients suffering from uveal melanoma, is the fractionated stereotactic radiotherapy (SRT). It benefits in increasing tumor control and less toxicity. For this method linear accelerators (LINACs) are used applying 4 – 5 fractions with a total dose between 50 and 70 Gy [14].

Before stereotactic photon beam radiosurgery as well as radiotherapy is applied no preliminary surgery is necessary for locating the tumor and its boarders. This is either done by computer tomography (CT) or magnetic resonance imaging (MRI) or a combination of both modalities. For illustrating the tumor volume a three-dimensional array is used, which enables the alignment of the treatment beams. If the treatment coordinates are derived once it is of a great importance that the tumor, with respect to the head frame, stays always at the same position during the dose delivery. As it is very difficult for the patients to not move the eye, an eye fixation aid is used which attaches to the head frame. For being able to monitor the reproducibility of the eye position, an eye tracking system has been developed too [14], [24].

Stereotactic photon therapy is preferably used for treating larger uveal melanoma. Some studies have shown that in this case it is effective for eye- and visual preservation [25].

1.4.4. Brachytherapy of ocular tumors

The first time ocular tumors have been treated by brachytherapy has been by Foster Moore in 1930 who used radon seeds. Following him Stallard used these radon seeds to treat patients suffering from retinoblastoma and suggested in 1939 to use cobalt-60 instead. The first time when Stallard started to use cobalt plaque brachytherapy for treating uveal melanomas was in 1950. Cobalt was in use for a long time till it was found out that the high energy of cobalt-60 implicated some unwanted biological effects. At the same time several other isotopes were introduced but only ruthenium-106 and iodine-125 remain to be commonly used nowadays [26].

The treatment of ocular tumors with ^{106}Ru and ^{125}I COMS plaques offers the big advantage of the short effective range of a few millimeters of both, the electrons and the photons. This

bases on the energy of a few MeV of the beta particles that are emitted by the ^{106}Ru plaque as well as the very low energy of a few keV of the photons of the ^{125}I COMS plaque [27], [28].

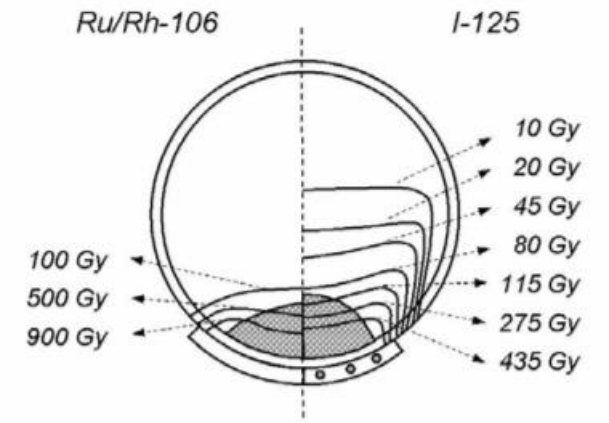

Figure 4: Contrasting juxtaposition of the isodose curves of the ^{106}Ru and ^{125}I COMS plaque (from [20]*).*

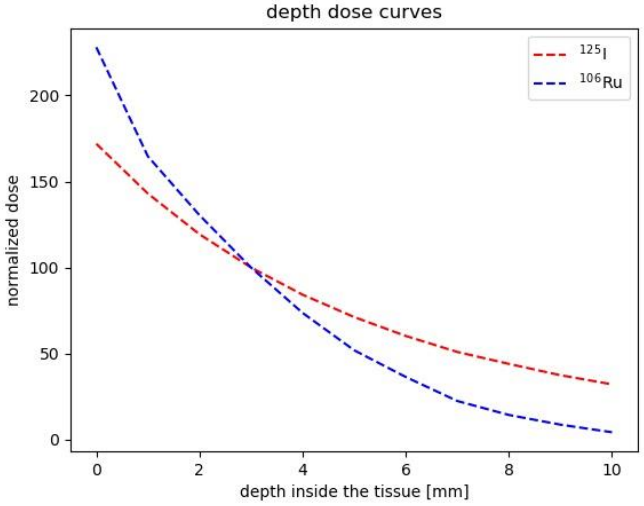

Figure 5: Depth dose curves of ^{125}I and ^{106}Ru. The x-axis indicates the depth in the tissue measured in millimeters and the y-axis shows the dose values normalized to the one in a 3 mm depth. It can be seen that the absorbed dose at the entrance of the tissue using ^{106}Ru is higher compared to the one using ^{125}I, but therefore it is declining rapidly. This way the distant parts of the tissue are absorbing more dose if ^{125}I is used.

1.5. Difference between ^{106}Ru plaques and ^{125}I COMS plaques

For the treatment of patients suffering from uveal melanoma temporary surface plaques, such as ^{106}Ru and ^{125}I COMS plaques are applied. These two are the most prominent one, while the ^{106}Ru plaques are preferably used around Europe and ^{125}I COMS plaques are used within the United States [26], [29].

1.5.1. ^{106}Ru eye plaque

The quite rare chemical element ruthenium has a few isotopes including ^{106}Ru. The half life time of ^{106}Ru is 368.2 days and it decays according to the law of radioactive decay

$$N(t) = N_0\, e^{-\lambda t} \qquad (2)$$

to ^{106}Rh. During this first step beta particles which have a maximum energy of 0.039 MeV (mean energy 0.01 MeV) are emitted. ^{106}Rh then decays with a half-life time of 2.2 h into the stable isotope ^{109}Pd also emitting beta particles with a maximum energy of 3.54 MeV (mean energy 1.43 MeV). These electrons have a low range and therefore enable the sparing of the surrounding, non-tumorous tissue. Furthermore the radiation protection of the personnel is simplified due to this low range [26], [27], [29].

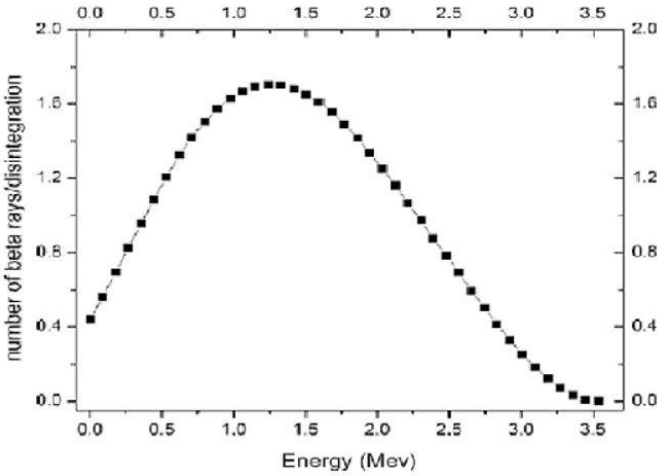

Figure 6: Energy spectrum of 106 Ru/ 106 Rh (from [30]*).*

The first one introducing the ^{106}Ru eye plaques was Prof. Peter Lommatzsch who started to use these applicators for treating uveal melanomas in 1964. In a first step he applied it during the treatment of choroidal melanoma, followed by the ciliary body melanoma.

The company Eckert & Ziegler BEBIG GmbH located in Berlin, Germany produces these ^{106}Ru plaques since the 1990s [26].

The radionuclide ^{106}Ru is applied on a thin silver foil by electrolysis and then further placed on a 0.9 mm thick silver plate. The concave and convex side of the applicator show different properties. The concave side is provided with an additional, thin silver sheet of 0.1 mm, called exit window, covering the ^{106}Ru layer and resulting in almost no absorption of the beta particles. The silver layer of 0.7 mm covering the ^{106}Ru layer on the convex side of the applicator results in an absorption of more than 95% of the radiation [20], [26], [27].

The plaque is available in several different shapes and sizes. The diameter can vary from 11 to 25.4 mm with a spherical radius of 12 - 14 mm. The ^{106}Ru plaques have an inactive edge of between 0.7 mm and 0.8 mm at the peripheral margin of the plaque. Besides the round applicators which are preferably used treating uveal melanomas there are also some including small notches on one side of the applicator. These notches make it possible to place the plaque near the optic nerve head to treat juxtapapillary tumors. In addition to that there are some other geometries like crescent-shaped applicators. They can be used for treating tumors in the anterior region of the eye involving the ciliary body and/or the iris periphery and make it possible to spare the cornea. These different geometries bring along different activities varying between 10 – 25 MBq. This results in a dose rate of about 80 – 120 mGy/min at a reference depth of 2 mm from the plaque surface. Based on the half life of ruthenium these applicators can be used for 1 to 1.5 years [20], [26], [27].

Figure 7: Different sizes and geometries of the ^{106}Ru plaques. In row one and two the normal round plaques can be seen. The third row shows the plaques including the small notches that allow the placement of the applicators near the optic nerve head. Row number four depicts the crescent-shaped plaques (from [26]*).*

1.5.2. ^{125}I COMS plaque

^{125}I was discovered by Allen Reid and Albert Keston in 1946 but was firstly used within brachytherapy 20 years later. The production of ^{125}I is based on the reactor irradiation of ^{124}Xe. ^{125}I itself is a gamma emitter decaying with a half life time of 59.4 days according to equation (2) to the first excited state of ^{125}Te by electron capture. In a next step ^{125}Te, which is not a

metastable state, de-excites to its ground state by emitting a single gamma ray of an energy of 35.5 keV and an intensity of 7%. Besides this gamma ray a few characteristic x-rays in the range of 27 to 32 keV are produced by internal conversion. 1.4 photons with an energy greater than 10 keV are averagely emitted per disintegration. The electrons that emerge with an intensity of 2% by electron capture have a maximum energy of 35 keV, which is low enough to be absorbed by the iodine itself and the material of the capsules holding the seeds. In addition to that also the low mean energy of the arising photons (28 keV) is easily shielded by a 0.03 mm half value layer of lead. This enables an easier radiation protection. Based on its long half lifetime ^{125}I suits perfectly for temporary and permanent implants [20], [28], [31], [32].

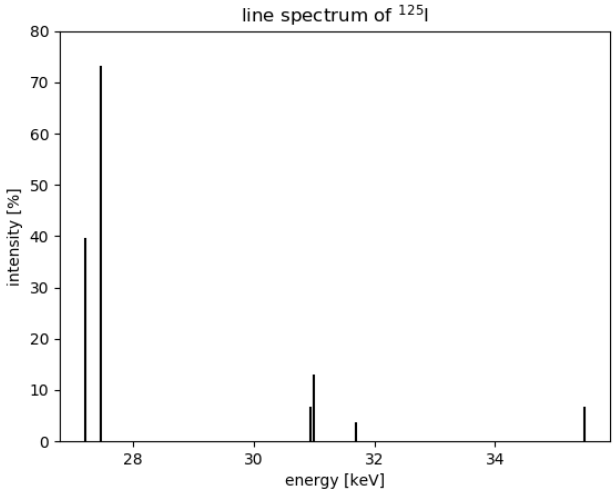

Figure 8: Line spectrum of ^{125}I.

The two main components of the standard ^{125}I COMS plaque are a gold-alloy backing (trade name Modulay) and a Silastic (MDX4-4210 bio-medical grade elastomer; Dow Corning Corp., Midland, MI) seed carrier insert. Depending on the usage they can differ in size varying from 10 to 22 mm in diameter with 2 mm increments. The ^{125}I seeds that are mostly placed inside titanium capsules are embedded in the grooves on the convex side of the Silastic insert. The number of the seeds, that are arranged in polygon rings, varies between 5 to 24 according to the size of the plaque, as shown in Figure 9. The placement of the seeds within the slots can be chosen individually, according to the treatment plan and the loading diagram. For a better fixation of the plaque to the eye there are some suture lugs on one side of the applicator [20], [21], [33].

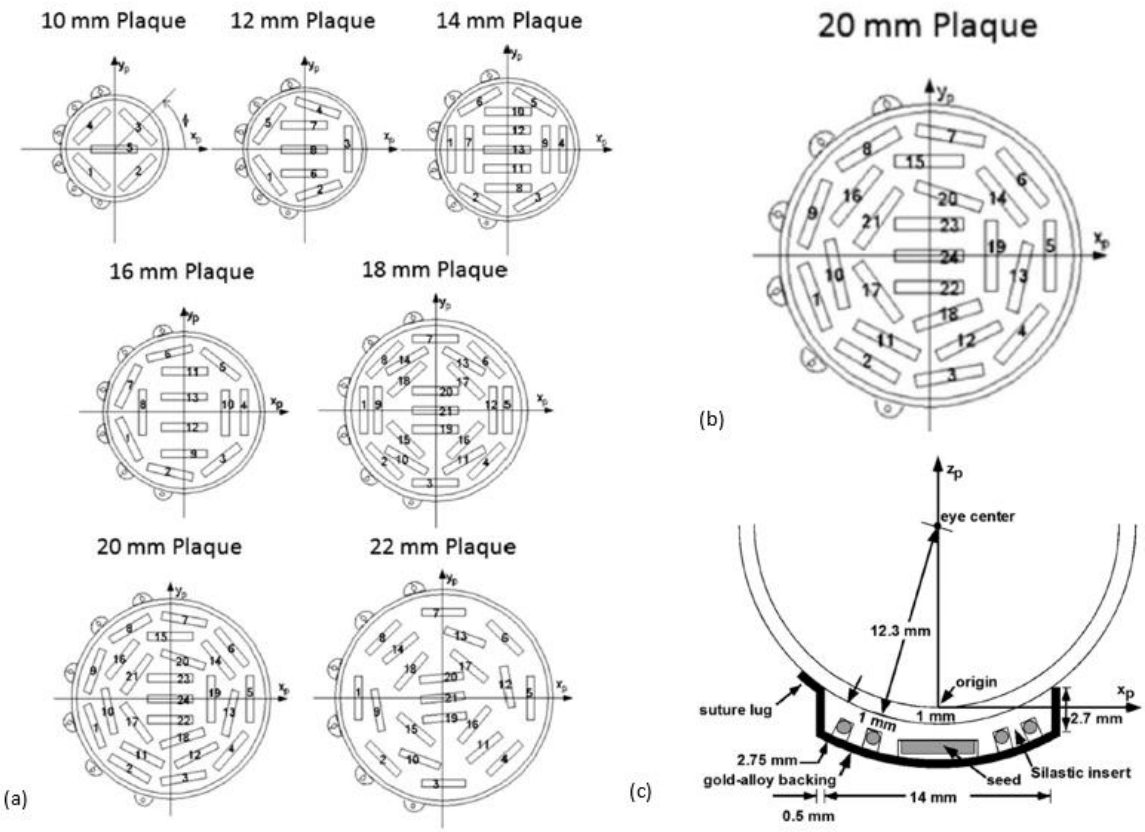

Figure 9: (a) Different sizes of the ^{125}I COMS plaque including their corresponding number and order of the seeds. The z_p-axis is pointing into the drawing plane. (b) Image of the x_py_p-plane of the 20 mm plaque. (c) Showing the x_pz_p-plane of the 14 mm COMS plaque (from [21]*).*

1.6. Purpose of this work

The purpose of this work was to extend an existing scientific treatment planning software for ^{106}Ru eye plaque brachytherapy to include ^{125}I COMS plaques.

Heilemann *et al.* [27] already developed a treatment planning software capable of dose calculation, to compare the two different treatment modalities, the CCA and CCB ^{106}Ru plaque. In addition to that an anatomically accurate 3D model of the eye using the 3D animation software Houdini FX (Side Effects Software Inc., Toronto, Canada) has been incorporated too by Heilemann *et al.* [34]. This model includes anatomical structures like the lens, ciliary body, optic nerve, macula choroidea, cornea as well as the retina and sclera. The dome-shaped tumor that has been included in this model, can be varied in diameter and apex height. The geometrical models of the different ruthenium plaque types CCA, CCB and COB that have been integrated too, base on the ones produced the Eckert & Ziegler BEBIG GmbH located in Berlin, Germany.

Using Monte Carlo simulations some dose lookup tables have been generated for each single plaque type. Furthermore, a voxelized eye model overlaying the lookup tables, that have been generated by the MC simulation was used. Therefore, a certain number of

200 x 200 x 200 μm^3 voxel was assigned to every part of the eye. This superposition enabled a comparison of the different dose distribution based on the single plaque types and the resulting effect on the tumor

The MC generated ^{125}I dose lookup tables by Buzatu [35], were reviewed in a previous thesis project by myself. In frame of this unpublished work [36] some errors were observed, showing that the seeds haven't been aligned in the correct way, according to graph (b) in Figure 9. For being able to simulate some dose calculations these erroneous dose lookup tables need to be fixed as part of this master thesis and included into the 3D animation software Houdini FX (Side Effects Software Inc., Toronto, Canada). Additionally, to the revision of the ^{125}I dose lookup tables a 3D representation of the shape of the ^{125}I COMS plaque was already incorporated in the 3D animation software Houdini FX in the unpublished work [36] by myself, which should now be adapted according to the exact geometrical parameters that are mentioned in the TG 129 report [21].

Based on the existence of the geometrical model for the different types of the ^{106}Ru plaques and the ^{125}I COMS plaque as well as the implemented dose look up tables the purpose of this master thesis is to compare these different treatment methods dosimetrically by examining the impact on the treatment planning, dose-optimization and different exposure of the organs at risk (OAR). This is done for different tumor geometries and eye geometries. This systematic comparison should be helpful for developing recommendations for the most optimal selection of the applicators and subsequent treatment planning.

2. Material and Methods

^{125}I dose lookup tables that were generated by Buzatu [35] using MC simulation, were implemented in the frame of this master project in an already existing treatment planning software that was developed by Heilemann *et al.* [27]. This way dose calculations for different tumor configurations and positions inside the eye were done. Therefore, a geometrical 3D model of the 20 mm COMS plaques was implemented in the 3D animation software Houdini Apprentice Non-Commercial 16.0.633 (Side Effects Software Inc., Toronto, Canada). This enabled the investigation of the tumor coverage and the absorbed dose of the OAR.

2.1. Monte Carlo generated dose libraries

The ^{125}I dose lookup tables of the bachelor thesis [35] generated with the Monte Carlo code MCNP were already revised by myself in the unpublished work [36]. As a result of this revision some errors in defining the active seed geometry of the simulated 20 mm ^{125}I COMS were discovered. They had to be corrected for being able to compare both modalities, the ^{106}Ru plaques and the ^{125}I COMS plaque.

During a further investigation of the erroneous MC generated ^{125}I dose lookup tables of the bachelor thesis [35] it was found out that there was a bug in the calculation of the mesh bins of MCNP's *f4 tally which was corrected. The corrected values were placed at the same depth and again converted to Gy, using the respective f6 tally value along the central axis as calibration factor for all mesh bins at the same depth. In addition some input data of the Matlab code from the preceding bachelor thesis [35], that was used for the normalization of the whole *f4 tally, using MatlabR2016 MathWorks were adapted. The normalization process was done for each of the 24 *f4 tally resulting in the final dose lookup tables of each seed.

These Excel files, again included 150 matrices in the shape of (150 x 150), each matrix representing one out of the 150 layers the plaque was divided to, with a thickness of 0.02 cm. The shape of the square with its dimension of 29.8 x 30.0 x 29.8 mm^3 (length x depth x height), the ^{125}I COMS plaque was centered in and the voxel size of 200 µm, that were used by Buzatu [35] for simulating the lookup tables were not changed. Also the composition of the seed itself, such as the radioactive layer, the silver rod, the gas cavity and the titanium shell stayed the same as in the preceding bachelor thesis [35]. Together with the activity in Becquerel and the irradiation time in seconds these lookup tables, that are given in Gy/decay, represent the absorbed dose of the tissue.

2.1.1. Reviewing of the data

To make sure that after modifying all these files there wasn't any error left, these new normalized dose lookup tables were reviewed by plotting them visually. This screening of the data was done with the same python code that was used in the unpublished work [36] before. It saves one plot of every single layer out of the 150 ones the plaque was sliced into. Using the image processing software ImageJ (National Institutes of Health version, Bethesda, Maryland, United States) these 150 plots were stacked together. The resulting 3D image of the plaque could now be scrolled through, inspecting the dose distribution of every single layer. This way the symmetry and consistency of the dose distribution could be reviewed with the specified plaque and seed geometry as depicted in Figure 9.

2.1.2. Implementing the dose lookup tables into the 3D software

After validating the data, these new normalized dose lookup tables were converted into npz-files (a standard binary file format in Python) using Python 2.7.14. This allowed to implement the dose matrices into the 3D animation software Houdini Apprentice Non-Commercial 16.0.633 (Side Effects Software Inc., Toronto, Canada).

As mentioned in section 1.5.2 the slots of the ^{125}I COMS plaque can be filled individually with the seeds according to the treatment plan and the loading diagram. The simulation of this individual treatment method was facilitated by the implementation of 24 toggle boxes by myself in the unpublished work [36], each representing one seed, that can be ticked on demand. Hence, each dose lookup file out of the 24 was converted separately by using the same python script as in the unpublished work [36], which reads them one by one, stacking the 150 individual 2D dose planes (size 150 x 150), resulting in a 3D matrix with the dimension of (150, 150 ,150). Like in the unpublished work [36] the 24 resulting npz-files represent the overall dose distribution of every single seed within the plaque as a whole, not sliced into single layers anymore.

2.2. Adapting the treatment planning systems for ^{125}I COMS plaques

2.2.1. Houdini

Houdini FX (Side Effects Software Inc., Toronto, Canada) is a 3D animation software that enables the user to create geometric objects by connecting different functional nodes. Inside these nodes different actions, such as creating boxes or spheres and cutting them etc., are stored. They are connected to each other like a network and pass on their information from the top to the bottom. These nodes are created in the so-called geometry level which is subordinated to the object level. If the information of the geometry level reaches the bottom it is pulled up to the next higher object level to perform the required action.

Additionally, to the opportunity to create singles actions and save them individually, it is also possible to include Python (Python Software Foundation, Beaverton, USA) into Houdini FX by creating a python node. This enables the user to directly write a required python code inside there to affect the geometry.

2.2.2. Eye model

As mentioned in section 1.6 there was already an eye model including the OAR, such as the optic nerve, the macula, the cornea, the lens, the ciliary body, the sclera, the choroidea and the retina, developed in the 3D animation software Houdini FX (Side Effects Software Inc., Toronto, Canada) by Heilemann *et al.* [27] (Figure 10).

Based on Figure 9 from TG 129 report [21], which served as a template for the geometry of the ^{125}I COMS plaque, the eye radius in this study was assumed to be 12.3 mm instead of 12 mm that were used for the simulation for the ^{106}Ru plaques. Therefore, the eye radius itself, the radius of the different eye skins (sclera, choroidea and retina) and the other OAR as well as their distances to each other were modified according to the 12.3 mm. This was solved by including a new variable global parameter that could be changed manually by typing in the required value and linking it to all the eye skins and the other OAR to enable an automatic adjustment of them according to the value that is entered.

Table 1: Parameters of the OAR that were used for the simulated eye model within the 3D animation software Houdini FX (Side Effects Software Inc., Toronto, Canada).

organ	radius [mm]	thickness [mm]
sclera	12.3	1.0
choroidea	11.3	0.2
retina	11.1	0.4
cornea	8.3	0.5
ciliary body	6.5	1.0
lens	4.0	2.25
macula	2.0 – 4.0	0.4
optic nerve	1.0	-

The dome-shaped model of the tumor that was already used in the preceding master thesis [1] was adjusted too according to the newly included global variable. Thus, the size of the tumor, which is defined by the apex height and the diameter, was linked to this new parameter. This way the size ratio of the tumor to the eye changes simultaneously with the typed in value of the global parameter. Furthermore, also the position of the tumor was

adjusted by changing the distance to the xy – surface in which the eye model was placed. Since the eye radius of the ^{125}I COMS plaque study was 0.3 mm larger than in the ^{106}Ru plaque study the distance to the xy – surface had to be shortened.

The size of the tumor itself can still be varied by adjusting the diameter, consisting out of two parameters, and its apex height. Since the investigations of this thesis are only related to tumors with a circular profile and not an elliptical one, both diameter parameters always had the same value.

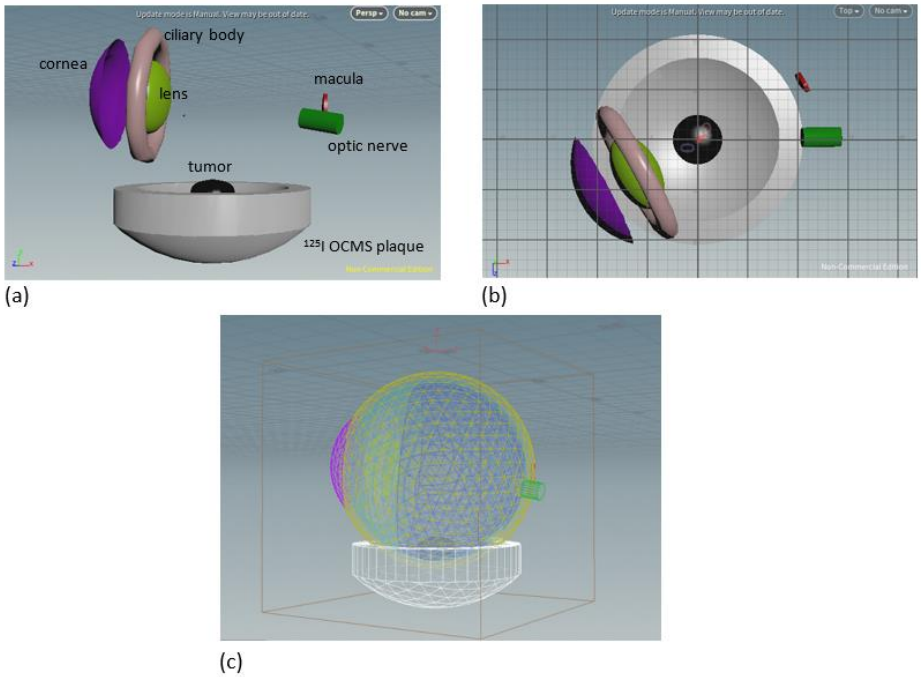

Figure 10: Screenshots of the 3D animation software Houdini FX (Side Effects Software Inc., Toronto, Canada). (a) shows the sideview and (b) the top view of the implemented 20 mm ^{125}I COMS plaque and the OAR, excluding the eye skins. Graph (c) depicts the whole eye model together with the 20 mm ^{125}I COMS plaque, also including the eye skins (sclera – yellow sphere; choroidea – light blue sphere; retina – dark blue sphere)

2.2.3. ^{125}I COMS plaque model

The COMS plaque model that is used within this master thesis has a diameter of 20 mm. The 24 seeds, that are arranged according to the illustration in Figure 9, are placed inside a silastic seed carrier that is surrounded by a gold-alloy backing. The silastic seed layer between the bottom row of the seeds and the eye is about 1 mm thick [21].

A geometrical model of this ^{125}I COMS plaque was already developed in the unpublished work [36], by copying one of the existing architectures of the three ruthenium plaques and adapting it for the 20 mm ^{125}I COMS plaque.

As part of this master thesis this newly created architecture for the ^{125}I COMS plaque was adapted in detail in size and shape according to the parameters that are mentioned in the TG 129 report [21]. Some of the 20 mm ^{125}I COMS plaque parameters weren't given and had either to be calculated or measured by drawing a sketch of it. This was done by taking graph (c) of Figure 9, showing the parameters of the 14 mm ^{125}I COMS plaque, as a template and using the mathematical formulas of the circular segment to recalculated the correct values of the missing parameters of the 20 mm ^{125}I COMS plaque. The center of the plaque aligns with the center of the eye, therefore the angle was calculated resulting in a value of 54.4°. It is the angle between the vertical line in the middle of the eye and the edge of the plaque.

After calculating all these missing parameters, they were used for the construction of the geometrical model of the 20 mm ^{125}I COMS plaque within the 3D animation software Houdini FX (Side Effects Software Inc., Toronto, Canada). For this construction different geometrical shapes of different sizes were combined and cut on the right place resulting in the final 20 mm ^{125}I COMS plaque model depicted in Figure 11.

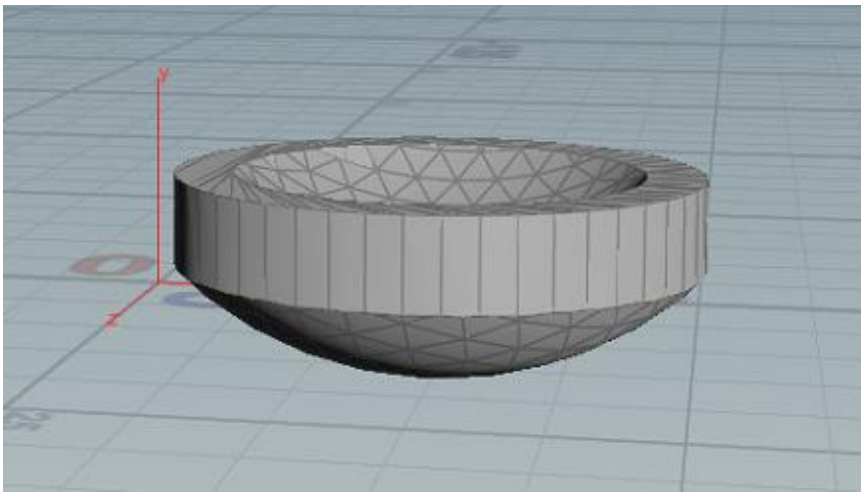

Figure 11: Screenshot of the developed 20 mm ^{125}I COMS plaque model.

2.2.4. Graphical user interface of the treatment planning software

The graphical user interface (GUI) of the 3D animation software Houdini FX enables the manual setting of some important parameters that are essential for the simulations. The interface is separated in three different tabs:

a. dose parameter
b. tumor parameter
c. COMS

Inside the dose parameter tab (Figure 12) the prescribed dose in Gray (Gy), the activity in MBq (megabequerel) and the resident time in minutes can be set. Further down are some check boxes each representing one OAR. By ticking them the dose volume histograms (DVH)

are calculated and the values are saved as individual npz-files. Additionally, it can be chosen whether the displacement calculations should be included too in the simulations by ticking the check box named error DVH. If so a drop down menu opens in which the required volume coverage, given in percentage, can be typed in.

The tumor tab (Figure 13) includes all the parameters describing the plaque type, the eye and the tumor itself. The plaque index, the tumor apex height, the two tumor basal diameters, the eye radius as well as the distance of the tumor to the macula and the optic nerve can be modified. All these parameters besides the plaque index are measured in millimeters. If the error DVH check box in the dose parameter tab is ticked the desired value of the plaque shift, measured in millimeters too, can be typed in in the error check box of the tumor parameter tab. Scrolling further down in this tab also the calculated $D_{2\%}$, $D_{98\%}$, D_{mean} values of all the before selected OAR, whose DVH check boxes are ticked in the dose parameter tab, and the tumor as well as the apex dose, the V_{95}, V_{90}, D_{max} and D_{min} values of the tumor are displayed. If the error calculations are included too in the simulations, a new menu pops up showing the calculated apex dose, $D_{2\%}$, $D_{98\%}$ and D_{mean} values of the tumor, and the minimum and maximum $D_{2\%}$ and D_{mean} values of the displacement for every single selected OAR.

The last tab named COMS (Figure 14) includes the 24 toggle boxes, each representing one single seed of the 20 mm ^{125}I COMS plaque, that can be ticked on demand and hence enables the simulations of individual treatment methods.

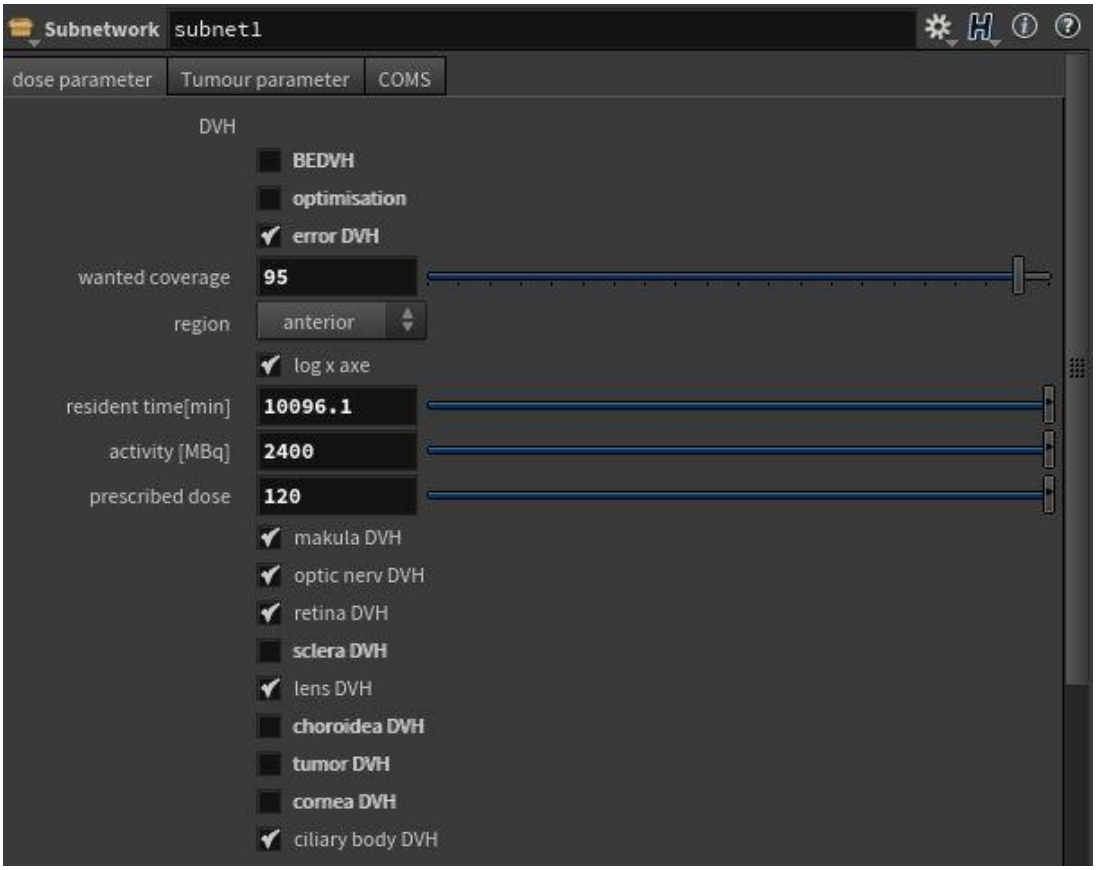

Figure 12: Screenshot of the GUI displaying the dose parameter tab listing all the dose specific parameters that can be adjusted manually.

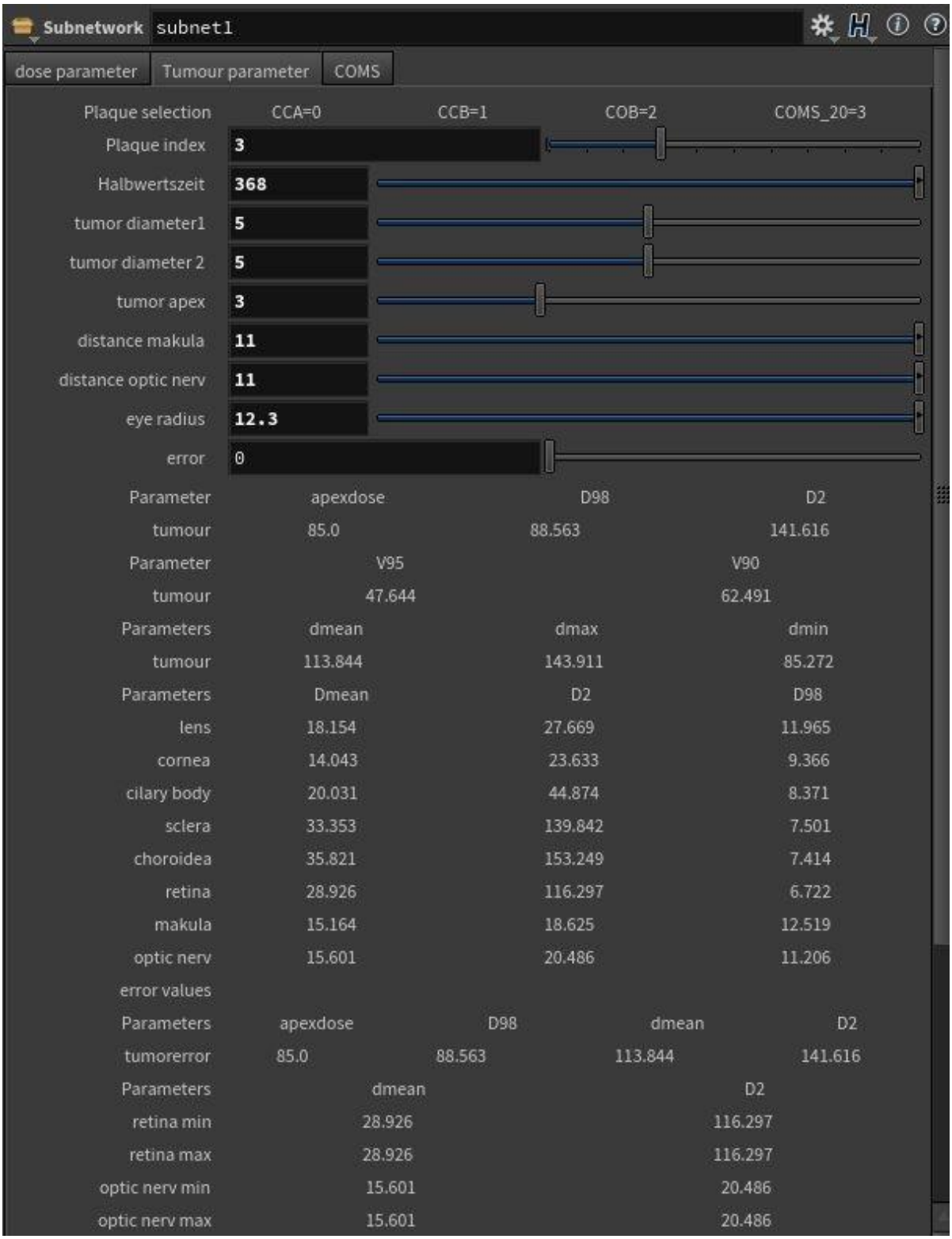

Figure 13: Screenshot of the GUI showing the tumor parameter tab enabling the adjustment of the tumor parameters. In addition, the plaque type can be selected and its displacement can be modified. It also displays the calculated dose values of the OAR and the tumor.

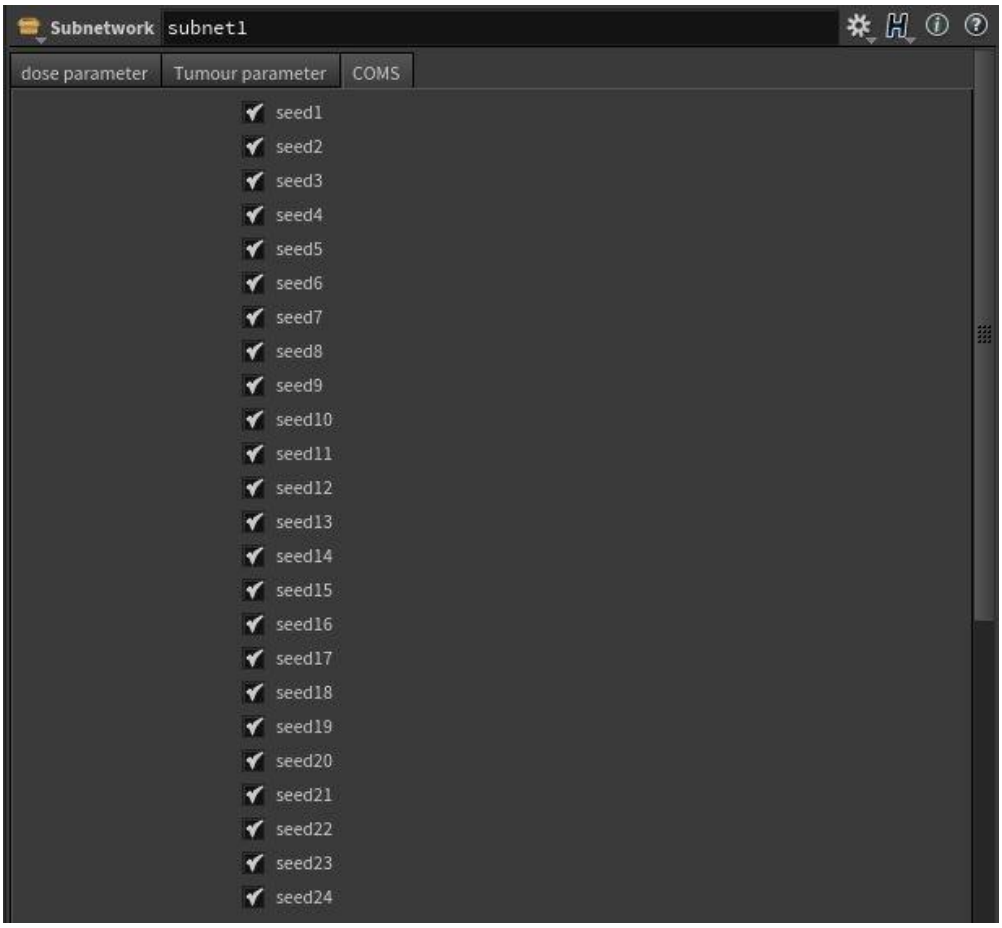

Figure 14: Screenshot of the GUI of the COMS tab including the 24 toggle boxes each representing one seed of the 20 mm ^{125}I COMS plaque that can be ticked on demand.

2.3. Dosimetric consideration of ^{125}I COMS plaques

2.3.1. Tumor Coverage

For getting an overview of the possible scenarios in which the tumor receives enough dose to be efficiently treated, considering different tumor locations, tumor diameters, apex heights and displacements, the tumor coverage was investigated calculating V95. This was done by using the npz-files, including the resulting dose volume histogram (DVH), that were generated for every single tumor configuration. V95 indicates the percentage of the tumor volume that receives at least 95% of the prescribed dose. The ideal value of V95 is 100%. If it drops below 100%, for the sake of this study it is assumed that this configuration wouldn't be efficient enough in treating the tumor.

As part of this master thesis the tumor coverage of two different ^{125}I COMS plaque configurations was reviewed. The first configuration was the fully occupied ^{125}I COMS plaque. All the 24 grooves were filled with radioactive seeds. This plaque will further be referred to as Plaque1. The second configuration that was used for this study was the ^{125}I COMS plaque filled

with the grooves 10 – 24 according to Figure 9, sparing the outer ring (groove 1 to 9). This Plaque is denoted as Plaque2 throughout this master thesis.

For the investigation of the tumor coverage the dose which the OARs receive, was not of interest. Therefore, the tumor could be placed anywhere inside the eye. In this master thesis the central position with a fixed distance of 11 mm to the optic nerve and the macula, as can be seen in Table 4 and Figure 15, was chosen. Not only the neutral position of the plaque, in which the center of the plaque aligns with the center of the eye, was of interest, but also some displacement of the plaque relative to the tumor, that can occur due to imperfect positioning of the plaque during surgery (1 mm and 2 mm displacement). For all of these three different displacements the diameter of the tumor was varied in 1 mm steps starting from 5 mm and finishing with 20 mm, while its apex height was increased from 3 mm to 8 mm in 0.5 mm steps. The prescribed dose was 85 Gy to the apex of the tumor throughout this investigation. The resident times for the different apex heights were calculated manually and are listed in Table 2. For all of these simulations the same activity of 2400 MBq was used. If not all the grooves of the plaque were filled with radioactive seeds the activity of 2400 MBq was split between the filled ones. For Plaque1 this resulted in an activity of 100 MBq per seeds, whereas using Plaque2 each seed had an activity of 160 MBq. These data were taken from a fact sheet of the Eckert & Ziegler BEBIG GmbH located in Berlin, Germany [37].

Additionally to V95 also the $D_{98\%}$, called the near minimum dose, which states the coolest 98% of the tumor volume and therefore is the minimum dose which 98% of the tumor volume receive, was calculated for all the above mentioned scenarios.

For each simulation of these scenarios a npz-file of the resulting DVH was saved. These individual files were further used to calculated the $D_{98\%}$ value. Based on the chosen step width of 0.01 mm of the resulting dose values, the output files of the tumor did not always include the exact 98% tumor volume value. Thus, a python script was written using the linear interpolation equation (3) searching for the next higher and next lower dose value surrounding the dose value that 98% of the tumor volume receive, to calculate it.

$$x = \frac{(y - y_1)(x_2 - x_1)}{(y_2 - y_1)} + x_1 \qquad (3)$$

Table 2: Detailed list of the parameters, including the apex height, the tumor diameter and the corresponding resident time that were used for the calculations of the first plaque configuration Plaque1 in the neutral position (displacement 0 mm) and the displacement positions of 1 mm and 2 mm. All 24 grooves were filled with radioactive seeds.

Plaque1								
displacement 0 mm			**displacement 1 mm**			**displacement 2 mm**		
apex height [mm]	**tumor diameter [mm]**	**resident time [min]**	**apex height [mm]**	**tumor diameter [mm]**	**resident time [min]**	**apex height [mm]**	**tumor diameter [mm]**	**resident time [min]**
3.0	5-20	10096	3.0	5-20	10176	3.0	5-20	10345
3.5	5-20	11016	3.5	5-20	11021	3.5	5-20	11144
4.0	5-20	11955	4.0	5-20	12049	4.0	5-20	12352
4.5	5-20	13073	4.5	5-20	13144	4.5	5-20	13348
5.0	5-20	14199	5.0	5-20	14347	5.0	5-20	14452
5.5	5-20	15385	5.5	5-20	15416	5.5	5-20	15572
6.0	5-20	16681	6.0	5-20	16886	6.0	5-20	16920
6.5	5-20	18043	6.5	5-20	18195	6.5	5-20	18347
7.0	5-20	19589	7.0	5-20	19610	7.0	5-20	19750
7.5	5-20	21100	7.5	5-20	21274	7.5	5-20	21402
8.0	5-20	22760	8.0	5-20	22806	8.0	5-20	23094

Table 3: Detailed list of the parameters, including the apex height, the tumor diameter and the corresponding resident time that were used for the calculations of the second plaque configurations Plaque2 in the neutral position (displacement 0 mm) and the displacement positions of 1 mm and 2 mm. The grooves of the outer ring 1 to 9 according to Figure 9 were spared and not filled with radioactive seeds.

Plaque2								
displacement 0 mm			**displacement 1 mm**			**displacement 2 mm**		
apex height [mm]	**tumor diameter [mm]**	**resident time [min]**	**apex height [mm]**	**tumor diameter [mm]**	**resident time [min]**	**apex height [mm]**	**tumor diameter [mm]**	**resident time [min]**
3.0	5-20	8983	3.0	5-20	9067	3.0	5-20	9311
3.5	5-20	9945	3.5	5-20	9973	3.5	5-20	10132
4.0	5-20	10964	4.0	5-20	11045	4.0	5-20	11398
4.5	5-20	12140	4.5	5-20	12215	4.5	5-20	12497
5.0	5-20	13357	5.0	5-20	13481	5.0	5-20	13700
5.5	5-20	14572	5.5	5-20	14771	5.5	5-20	14918
6.0	5-20	16007	6.0	5-20	16226	6.0	5-20	16212
6.5	5-20	17440	6.5	5-20	17642	6.5	5-20	17769
7.0	5-20	19081	7.0	5-20	19171	7.0	5-20	19349
7.5	5-20	20684	7.5	5-20	20812	7.5	5-20	21141
8.0	5-20	22443	8.0	5-20	22677	8.0	5-20	22797

2.3.2. Organs at risk

During the course of this master thesis the absorbed dose of the OAR using Plaque1 was investigated. For this study the tumor diameter was set to a fixed value of 5 mm, whereas the tumor apex height still varied in size (3, 5 and 8 mm). Compared to the study of the tumor coverage in section 2.3.1 in this study the position of the tumor inside the eye was of great importance, because the absorbed dose of the OAR differs depending on whether the irradiated tumor is placed close to or on the opposite side of them. Therefore, the anterior and posterior position of the tumor inside the eye, as depicted in Figure 15, were included too in this study. As with the central position, the anterior and posterior ones are also defined by a fixed distance to the macula and the optic nerve, see Table 4. The relative displacement of the plaque to the tumor varied from 0 - 2 mm in 0.5 mm steps and was inspected for all the three tumor locations (anterior, central and posterior). The dosimetric impact of these displacements was calculated for a rotation in both directions towards to and away from the OAR (-2 to 2 mm along the sclera). The activity was again set to 2400 MBq and the resident time that was necessary to get a prescribed dose of 120 Gy at the tumor apex was again calculated manually.

The same prescribed dose of 120 Gy at the tumor apex as in the case of the simulations with the ^{106}Ru plaques by Heilemann *et al.* [27] were used. This allowed a comparison of the resulting $D_{2\%}$ and D_{mean} values of each OAR of both modalities, the ^{125}I COMS plaque and the ^{106}Ru plaques.

The OARs that were inspected as part of this master thesis were the retina, the macula, the optic nerve, the lens and the ciliary body. For all of these OAR the absorbed dose was calculated separately for all of the above mentioned scenarios and saved as an individual npz-file.

The $D_{2\%,}$ called the near maximum dose, which states the hottest 2% of the tumor volume and hence is the maximum dose which 2% of the tumor volume receive, was calculated for all the above mentioned scenarios.

Therefore, the same python script as the one for the $D_{98\%}$ value calculation for the tumor mentioned in section 2.3.1 was used, but with the only difference that for the interpolation the next higher and next lower value surrounding the dose value that 2% instead of 98% of the tumor volume receive, was used.

The dose an organ receives on average (D_{mean}) of each single OAR was calculated taking the individual DVH that were saved as a npz-file for every single tumor configuration and applying another python script including equation (4) to them. The lower percentage volume value was subtracted from the higher one, weighing it with the corresponding dose value of the higher percentage volume value. The sum of all the N values was then divided by 100 indicating the whole organ volume of 100%.

$$D_{mean} = \frac{\sum_i^N (V_i - V_{i+1}) D_i}{100} \quad (4)$$

Table 4: This table gives an overview of the different positions of the tumor within the eye, which are defined by a certain distance to the optic nerve and the macula always measured from the edge of the tumor to the edge of the optic nerve and the macula.

position	distance to optic nerve [mm]	distance to macula [mm]
anterior	15	15
central	11	11
posterior	5	5

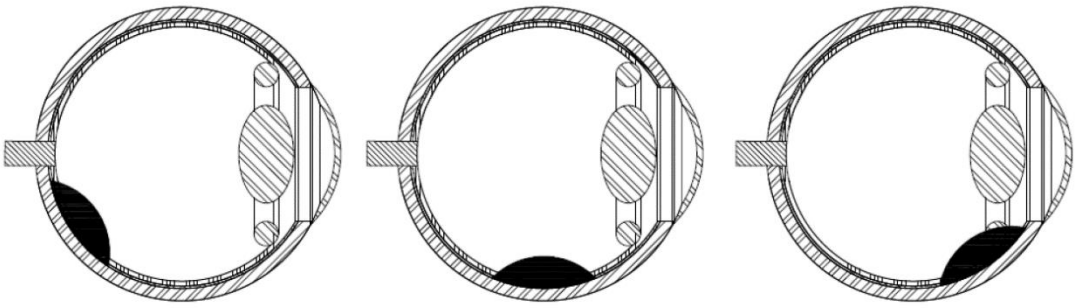

Figure 15: Schematic illustration of the different tumor positions within the eye according to Table 4. The posterior, central and anterior position from left to right (from [1]*).*

Table 5: Summary of the resident times for the different positions of the tumor within the eye (anterior, central and posterior) including the relative displacement of the plaque to the tumor (0, 1, 2 mm) and three different apex heights (3, 5, 8 mm) that were used for the calculations of the absorbed dose of the OAR using Plaque1.

Plaque1				
displacement [mm]	**anterior / central**		**posterior**	
	apex height [mm]	**resident time [min]**	**apex height [mm]**	**resident time [min]**
0	3	14253	3	15055
	5	20045	5	20700
	8	32131	8	32785
0.5	3	14304	3	15462
	5	20056	5	20987
	8	32367	8	33071
1.0	3	14366	3	15744
	5	20255	5	21435
	8	32196	8	33294
1.5	3	14548	3	16083
	5	20352	5	21830
	8	32462	8	33629
2.0	3	14605	3	16609
	5	20403	5	22314
	8	32603	8	33923

3. Results

3.1. Monte Carlo generated dose libraries

3.1.1. Reviewing of the data

As in the preceding unpublished work [36] a uniform colourmap indicating the different intensities of the dose distribution was used. This allowed to visualize the decrease of the dose with increasing distance to the seed on the concave side of the plaque. In the unpublished work [36] it was already shown that the plaque was laying perfectly in the center of the simulated square with the dimension of 29.8 x 30.0 x 29.8 mm^3.

Seed number 24 is located in the center of that plaque, as can be seen in Figure 9, which served as a template of the MCNP simulations in the preceding bachelor thesis [35]. This allowed visual screening of the data, as already be done in the unpublished work [36], and enabled an easier review of the correct seed position and the radial dose distribution. There are three different plots showing the radial dose distribution of seed 24 in three different views (Figure 16, Figure 17, Figure 18)

Figure 16 depicts the front view of the plaque (y_pz_p-plane according to Figure 9) showing the round profile of seed 24. Figure 18 illustrates the top view of the plaque (x_py_p-plane according to Figure 9) and Figure 17 shows the longitudinal dimension of the seed (x_pz_p-plane according to Figure 9). Taking a look at all these three figures (Figure 16, Figure 17, Figure 18) on the one hand side it can be seen that the seed is lying in the center of the plaque, as it should according to Figure 9, and on the other hand side these figures show the expected dose distributions.

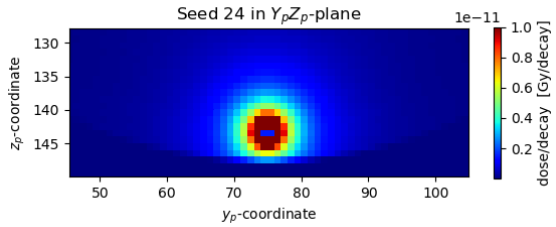

Figure 16: The front view of the plaque depicting the round profile of seed 24. The seed itself is the blue dot in the middle of the red circle. The numbers on the axes are indicating the 150 lines and columns in the matrix.

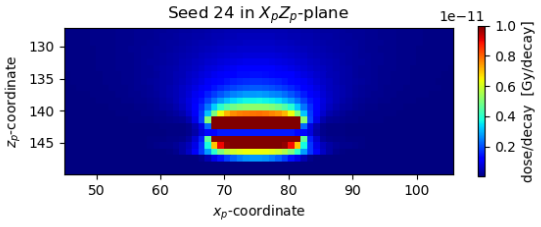

Figure 17: Longitudinal dimension of seed 24. Here the radial dose distribution, indicated by the red half circles can be seen. The seed itself is the blue line in between the red half circles. Again, the numbers on the axes are indicating the 150 lines and columns in the matrix.

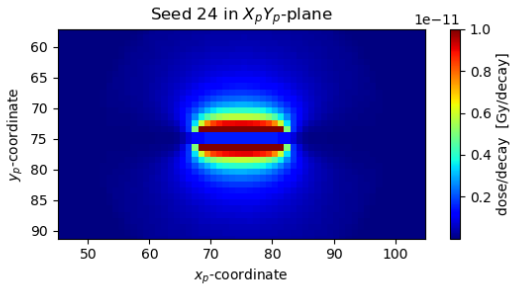

Figure 18: Top view of the plaque showing seed 24 lying exactly in the center of it (blue line in between the red half circles). The radial dose distribution, again indicated by the red half circles, can be perfectly seen too. Also, in this figure the numbers on the axes are indicating the 150 lines and columns in the matrix.

3.1.2. Implementing the dose lookup tables into the 3D software

The import of the dose lookup tables and calculation of the dose distribution of the ^{125}I COMS plaque differed to the one of the ^{106}Ru plaques that already existed. While the dose lookup tables of the ^{106}Ru plaques were directly read in as one whole npz-file, the final dose lookup table of the 20 mm ^{125}I COMS plaque first had to be calculated using a python code, with regard to the occupied grooves of the plaque. This code added up the individual generated npz-files of the seeds that were ticked inside the COMS tab and saved this sum as a new npz-file, that was used for further calculations.

For both, the ^{106}Ru plaque types CCA and CCB as well as the 20 mm ^{125}I COMS plaque the dose lookup tables were multiplied by the activity and the resident time resulting in the overall dose distribution. If the 20 mm ^{125}I COMS plaque is simulated and not all the grooves are occupied by radioactive seeds, the activity is distributed evenly to the seeds that are inserted.

3.2. Dosimetric consideration of ^{125}I COMS plaques

3.2.1. Tumor Coverage

As mentioned in section 2.3.1 we were interested in the tumor configurations whose V95 values equal 100%. If so, for sake of this study, these configurations were assumed to be efficient enough in treating the tumor.

The tumor coverage of the two different 20 mm ^{125}I COMS plaque configurations, Plaque1 and Plaque2, that were investigated for the central position of the tumor, showed different results.

The maximum tumor basal diameter that could be covered by Plaque1 differed according to the placement of the plaque. If the plaque was placed in the neutral position a tumor with a basal diameter of 16 mm could be covered, one of 13 mm for 1 mm displacement and one of 11 mm shifting it 2 mm away of the center. In all these cases the tumor apex height was 8 mm.

Plaque2 showed a less efficient coverage of the tumor resulting in a maximum apex height of 8 mm for all the displacements (0 mm, 1 mm and 2 mm), respectively, but a maximum basal diameter of 14 mm for the neutral position, 13 mm for 1 mm displacement and 10 mm for 2 mm displacement.

The investigation of the tumor coverage showed that the maximum basal diameter that can be efficiently covered by the prescribed dose is almost linear dependent on its apex height. Tumors with a lager apex heights allowed the coverage of wider basal diameters. On the contrary, smaller apex heights limited the coverage.

Table 6 gives a schematical overview of those tumor configurations whose V95 values equal 100%, including both Plauque1 and Plaque2.

Table 7 includes mathematical formulas which can be used to calculate the maximum basal diameter that guarantees the tumor coverage.

Figure 19 and Figure 20 show graphical illustrations of the change of the tumor coverage with regard to the apex height and the basal diameter of the tumor, generated using the values of Table 20 to Table 25 of Apex A.

Table 6: Overview of the optimal plaque selection. Ⅰ indicates Plaque1 filled with all 24 seeds and Ⅱ indicates Plaque2 with the spared outer ring (grooves 1 to 9 as depicted in graph (a) of Figure 9). If both plaque types are listed they would be both efficiently treating the tumor. If only one is listed the other one is not fulfilling the necessary conditions for the tumor coverage.

		neutral position		1 mm displacement		2 mm displacement	
apex height [mm]		**3.0 - 5.5**	**6.0 – 8.0**	**3.0 - 5.5**	**6.0 – 8.0**	**3.0 - 5.5**	**6.0 – 8.0**
tumor diameter [mm]	**5**	Ⅰ, Ⅱ	Ⅰ, Ⅱ	Ⅰ, Ⅱ	Ⅰ, Ⅱ	Ⅰ, Ⅱ	Ⅰ, Ⅱ
	6	Ⅰ, Ⅱ	Ⅰ, Ⅱ	Ⅰ, Ⅱ	Ⅰ, Ⅱ	Ⅰ, Ⅱ	Ⅰ, Ⅱ
	7	Ⅰ, Ⅱ	Ⅰ, Ⅱ	Ⅰ, Ⅱ	Ⅰ, Ⅱ	Ⅰ, Ⅱ	Ⅰ, Ⅱ
	8	Ⅰ, Ⅱ	Ⅰ, Ⅱ	Ⅰ, Ⅱ	Ⅰ, Ⅱ	Ⅰ, Ⅱ	Ⅰ, Ⅱ
	9	Ⅰ, Ⅱ	Ⅰ, Ⅱ	Ⅰ, Ⅱ	Ⅰ, Ⅱ	Ⅰ	Ⅰ, Ⅱ
	10	Ⅰ, Ⅱ	Ⅰ, Ⅱ	Ⅰ, Ⅱ	Ⅰ, Ⅱ	-	Ⅰ, Ⅱ
	11	Ⅰ, Ⅱ	Ⅰ, Ⅱ	Ⅰ	Ⅰ, Ⅱ	-	Ⅰ
	12	Ⅰ, Ⅱ	Ⅰ, Ⅱ	-	Ⅰ, Ⅱ	-	-
	13	Ⅰ	Ⅰ, Ⅱ	-	Ⅰ, Ⅱ	-	-
	14	Ⅰ	Ⅰ, Ⅱ	-	-	-	-
	15	-	Ⅰ	-	-	-	-
	16	-	Ⅰ	-	-	-	-
	17	-	-	-	-	-	-
	18	-	-	-	-	-	-
	19	-	-	-	-	-	-
	20	-	-	-	-	-	-

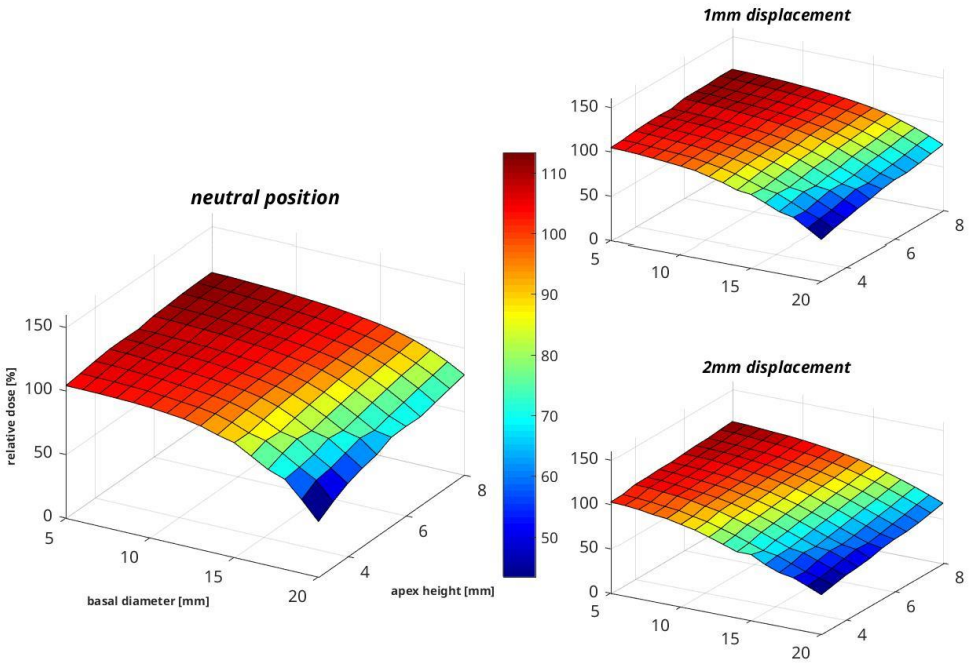

Figure 19: Change of the tumor coverage of Plaque1 as a function of the tumor basal diameter and its apex height. All three positions of the plaque relative to the tumor are depicted (neutral position, 1 mm and 2 mm displacement).

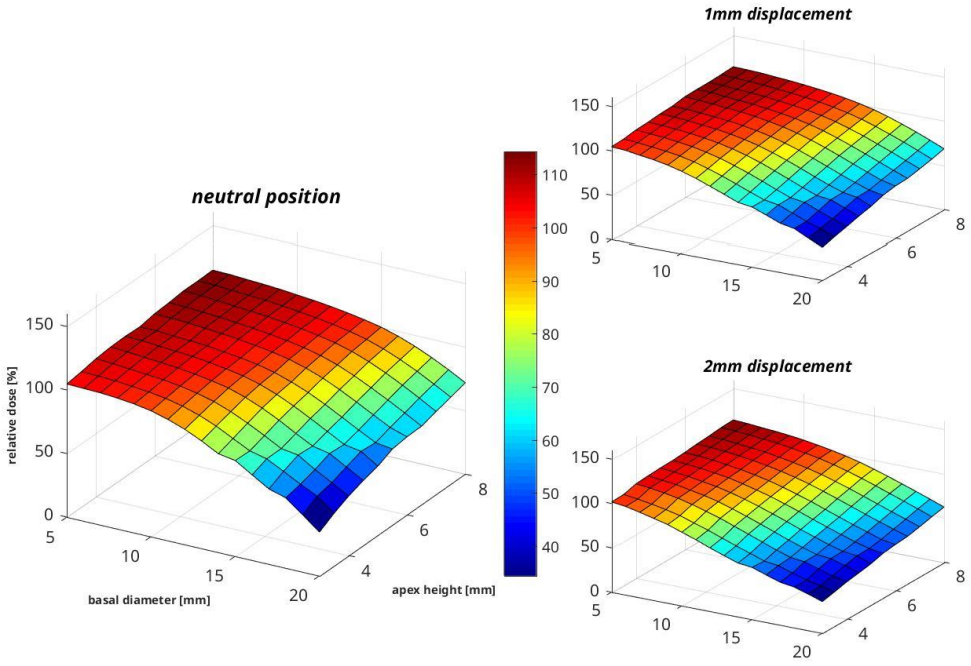

Figure 20: Change of the tumor coverage of Plaque2 as a function of the tumor basal diameter and its apex height. All three positions of the plaque relative to the tumor are depicted (neutral position, 1 mm and 2 mm displacement).

Table 7: Overview of the maximum treatable basal diameters D_{basal} for both observed plaque configurations Plaque1 and Plaque2 as a function of the apex height of the tumor H_{apex} for the neutral plaque position (0 mm displacement), 1 mm as well as 2 mm displacement.

Plaque type	displacements [mm]	maximum basal diameter [mm]
Plaque1	± 0	$D_{basal} \leq 11.2\,mm + 0.6\,H_{apex}$
	± 1	$D_{basal} \leq 5.8\,mm + 1.4\,H_{apex}$
	± 2	$D_{basal} \leq 4.4\,mm + 1.2\,H_{apex}$
Plaque2	± 0	$D_{basal} \leq 7.9\,mm + 0.9\,H_{apex}$
	± 1	$D_{basal} \leq 4.3\,mm + 1.3\,H_{apex}$
	± 2	$D_{basal} \leq 1.8\,mm + 1.4\,H_{apex}$

3.2.2. Organs at risk

When considering the serial OARs, such as the optic nerve, the macula or the lens, that are easily damaged if only a small part of it receives a high dose, the $D_{2\%}$ values were more important. For the parallel OARs, such as the retina, that still remain functional as long as not all the subunits are damaged, the D_{mean} value was highly relevant.

The accurate $D_{2\%}$ and D_{mean} dose values of the investigation are listed in Table 26 to Table 28. Using these values Figure 21 was generated which shows the respective dose values of different OARs for different tumor positions (anterior, central and posterior), including the plaque shifts from -2 mm to +2 mm. The negative displacement is a movement of the plaque away from the optic nerve, whereas the positive displacement describes a movement towards the optic nerve.

From the results of the simulations it emerged that the absorbed $D_{2\%}$ as well as the D_{mean} values of the individual OARs were increasing with an increasing tumor apex height.

Absorbed near maximum dose $D_{2\%}$ of the lens, the macula and the optic nerve for an anterior placed tumor

For an anterior position of the tumor the absorbed dose of the lens increased with shifting the plaque away of the optic nerve closer to the lens and decreased with moving the plaque towards the optic nerve. A comparison of the ^{125}I COMS plaque study with the previous one of the ^{106}Ru plaque study by Heilemann *et al.* [2] showed higher absorbed dose values of the lens for the ^{125}I COMS plaque, if tumors of an apex height of 3 and 5 mm were irradiated. The increase in dose was about 64% (44 Gy) and 54% (51 Gy) for ascending apex heights (3 and 5 mm) compared to the CCA plaque, and 17% (12 Gy) and 4% (4 Gy) compared to the CCB one.

On the contrary, the treatment of tumors with an apex height of 8 mm resulted in 7% (12 Gy) more dose using a CCA plaque and 46% (136 Gy) using a CCB one.

The absorbed $D_{2\%}$ values of the macula for an anterior located tumor and a neutral positioned plaque were almost 100% higher using the 20 mm ^{125}I COMS plaque. The dose differences between the 20 mm ^{125}I COMS plaque and the CCA as well as the CCB plaque were 15 Gy, 20 Gy and 32 Gy, for 3, 5 and 8 mm apex height, respectively.

For the optic nerve an increase of about 100% applying the 20 mm ^{125}I COMS plaque was observed too. The exact dose reduction if either a CCA or CCB plaque was used, was 17 Gy, 23 Gy and 38 Gy for an ascending apex height (3,5 and 8 mm).

Absorbed near maximum dose $D_{2\%}$ of the lens and the optic nerve for a central placed tumor

The investigation of the absorbed near maximum dose $D_{2\%}$ values of the lens and the optic nerve for a centrally located tumor and a plaque in the neutral position showed higher values for both OAR if any tumor configurations was irradiated with the 20 mm ^{125}I COMS plaque. Shifting the plaque towards the optic nerve its dose increased, whereas the ones of the lens decreased. The absorbed dose values using the neutrally placed 20 mm ^{125}I COMS plaque for irradiating tumors with an apex height of 3, 5 and 8 mm, were 98% (28 Gy), 97% (39 Gy) and 93% (61 Gy) higher for the optic nerve and 96% (37 Gy), 94% (52 Gy) and 87% (76 Gy) for the lens, compared to the ones using a CCA plaque. The increase of the absorbed $D_{2\%}$ values using the 20 mm ^{125}I COMS plaque compared to the ones of the CCB plaque was 91% (26 Gy), 90% (37 Gy) and 81% (53 Gy) for the optic nerve and 70% (27 Gy), 65% (36 Gy) and 31% (27 Gy) for the lens.

Absorbed near maximum dose $D_{2\%}$ of the macula, the optic nerve and the lens for a posterior placed tumor

If the tumor was placed in the posterior region of the eye in most of the cases, only with a few exceptions if the apex height of the tumor was 5 or 8 mm, the macula and the optic nerve absorbed more dose if a tumor was irradiated by the 20mm ^{125}I COMS plaque. A maximum for the absorbed dose of the macula and the optic nerve was observed for the neutral position of the plaque. The maximum value for the macula increased about 78% (52 Gy) and 71% (65 Gy), the one of the optic nerve about 64% (38 Gy) and 53% (43 Gy) if the 20 mm COMS plaque, instead of the CCA plaque, was used to irradiate tumors of an apex height of 3 and 5 mm, respectively. Using the 20 mm COMS plaque instead of the CCB plaque showed an increase of 40% (24 Gy) and 29% (24 Gy) of the maximum absorbed dose values by the optic nerve and one of 42% (54 Gy) and 31% (71 Gy) for the macula. Moving the plaque away as well as towards the optic nerve the absorbed dose values of the macula and the optic nerve in the ^{125}I COMS study resulted in a decrease of the absorbed dose by these two organs.

The situation is different for the lens. It showed a minimum for the neutral position and is increasing by shifting the plaque away and towards the optic nerve. Taking a look at the

absorbed $D_{2\%}$ values of the lens for a tumor located at the backside of the eye being irradiated by a neutrally positioned plaque, it can be seen that the values using a 20 mm ^{125}I COMS plaque are higher than the ones for the ^{106}Ru plaques CCB and CCA. Using a CCA plaque reduced the dose about 100%. The lens absorbed 28 Gy, 38 Gy and 60 Gy less for an apex height of 3, 5 and 8 mm, respectively. The dose reduction caused by the usage of a CCB plaque was about 96% (26 Gy), 95% (35 Gy) and 90% (54 Gy) for ascending apex height (3, 5 and 8 mm).

The averaged absorbed dose values D_{mean} and the near maximum dose $D_{2\%}$ values of the retina for a central placed tumor

The observation of the D_{mean} values of the retina yield increasing dose values with increasing apex height and a decreasing distance to the optic nerve for a central position of the tumor. The retina absorbed 65% (27 Gy) and 56% (31 Gy) less dose on average using a CCA plaque and 39% (16 Gy) and 29% (16 Gy) less using a CCB if tumors of an apex height of 3 and 5 mm were irradiated by neutrally placed plaques. On the contrary irradiating tumors of 8 mm apex height the lens on average absorbed less dose if the 20 mm ^{125}I COMS plaque was applied.

A comparison of the resulting absorbed near maximum dose values $D_{2\%}$ of the retina for a plaque in the neutral position showed that irradiating smaller tumors of an apex height of 3 mm resulted in higher values using the 20 mm ^{125}I COMS plaque. Whereas treating tumors of an apex height of 5 and 8 mm the retina absorbed more dose using one of the ^{106}Ru plaque types CCA or CCB. The values for the CCA one were 14% (38 Gy) and 63% (632 Gy) higher. The ones for the CCB were 9% (22 Gy) and 53% (424 Gy) higher.

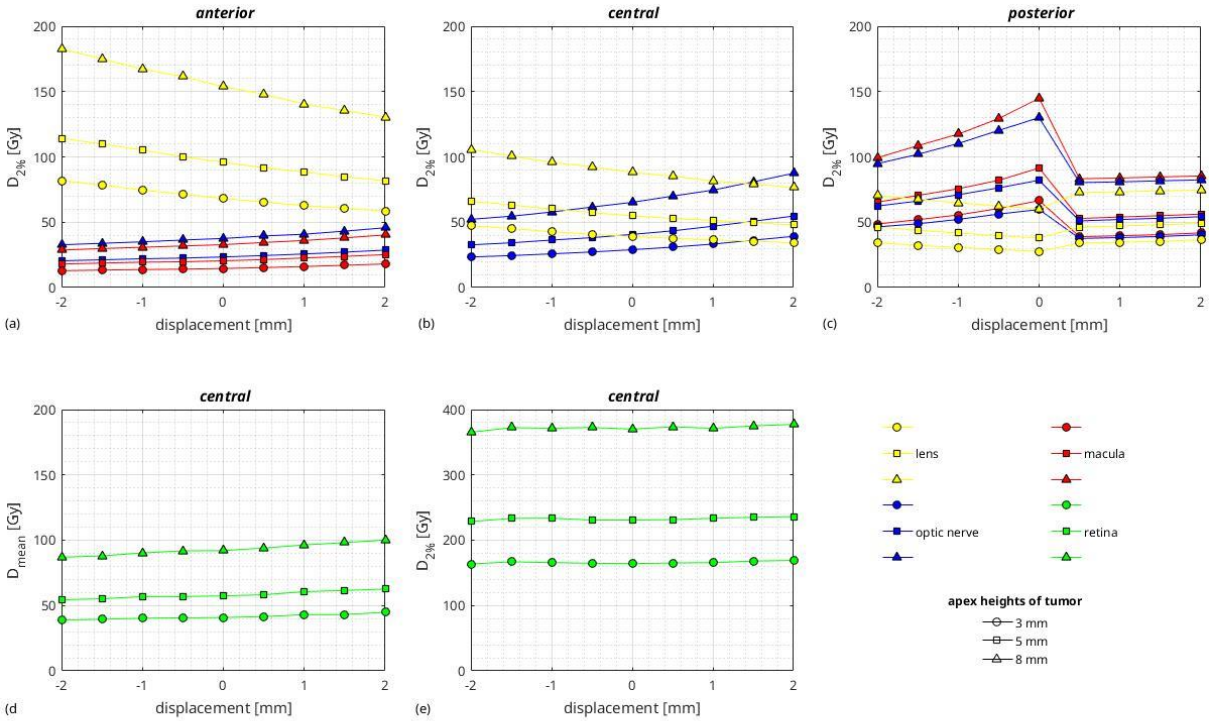

Figure 21: Absorbed dose values of selected OAR with regard to the different tumor positions, as depicted in Figure 15, and the simulated shifts of the plaque. (a) $D_{2\%}$ of the lens, the optic nerve and the macula for an anterior location of the tumor. (b) $D_{2\%}$ of the lens and the optic nerve for a central placement of the tumor. (c) $D_{2\%}$ of the lens, the optic nerve and the macula for a posterior positioned tumor. (d) showing D_{mean} and (e) depicting $D_{2\%}$ of the retina for a central tumor position.

Table 8 to Table 13 are giving an overview of the calculated difference between the dose values of the simulations with the ^{106}Ru plaque types CCA and CCB by Heilemann *et al.* [34] and the ones that were calculated for the 20 mm ^{125}I COMS plaque within this master thesis. The red values are indicating higher ^{106}Ru values. The values for the negative displacements (movement of the plaque away from the optic nerve) are listed in the columns headed min, whereas the ones of the positive shift (movement towards the optic nerve) are captioned max.

The anterior and posterior position of all three plaque types and the central position for the CCB and 20 mm ^{125}I COMS plaque were the same as listed in Table 4, only the distance for the central position of the CCA plaque differed in 1 mm. Instead of 11 mm distance to the optic nerve and the macula, 10 mm were chosen.

The computation of the dose values for the five OAR that were observed in the course of this master thesis took approximately 50 seconds.

Table 8: Calculated dose differences of the $D_{2\%}$ and D_{mean} values if the results of the ^{106}Ru plaque type CCA and the 20 mm ^{125}I COMS plaque are compared. In both simulations the tumor was placed in the central position, with the only difference that therefore a distance of 11 mm to the optic nerve and the macula was used for the 20 mm ^{125}I COMS plaque and one of 10 mm for the CCA plaque. The red values are indicating higher ^{106}Ru values.

			lens		optic nerve		macula		retina		ciliary body	
	error		$D_{2\%}$	D_{mean}	$D_{2\%}$	D_{mean}	$D_{2\%}$	D_{mean}	$D_{2\%}$	D_{mean}	$D_{2\%}$	D_{mean}
apex [mm]	0	3	37.4	25.4	28.2	21.8	25.7	21.2	14.5	26.7	56.2	27.1
		5	51.9	35.6	39.4	60.6	35.9	29.7	-38.3	32.0	76.3	37.7
		8	76.7	56.0	60.5	48.2	55.4	46.9	-632.0	-2.7	95.2	56.2

			min		max		min		max		min		max		min		max		min		max	
	error		$D_{2\%}$	D_{mean}	$D_{2\%}$	D_{mean}	$D_{2\%}$	D_{mean}	$D_{2\%}$	D_{mean}	$D_{2\%}$	D_{mean}	$D_{2\%}$	D_{mean}	$D_{2\%}$	D_{mean}	$D_{2\%}$	D_{mean}	$D_{2\%}$	D_{mean}	$D_{2\%}$	D_{mean}
apex height [mm]	0.5	3	38.8	26.2	36.3	24.7	26.7	20.8	30.0	23.1	24.1	20.1	27.2	22.4	15.6	26.2	15.6	26.5	58.6	28.3	54.2	26.3
		5	53.6	36.7	50.4	34.6	37.2	29.2	41.7	32.3	33.7	28.1	37.8	31.4	-37.5	31.0	-37.6	31-1	78.7	39.1	73.6	36.5
		8	78.8	57.9	76.0	55.0	58.1	46.5	63.8	51.0	52.8	44.9	58.4	49.5	-626.2	-4.5	-628.2	-7.0	93.6	57.8	97.0	55.4
	1	3	40.3	27.2	35.3	24.1	25.4	20.0	32.0	24.4	23.0	19.3	29.5	23.9	16.2	27.0	16.3	27.2	61.3	29.4	51.6	25.5
		5	55.8	38.2	49.3	33.9	35.6	28.0	44.7	34.3	32.4	27.1	41.2	33.6	-35.5	32.9	-35.3	32.1	82.2	40.8	71.0	35.7
		8	79.3	59.1	74.1	53.3	55.2	44.1	66.4	53.0	50.3	42.7	62.0	51.9	-630.5	1.4	-629.4	-9.8	88.8	58.3	94.7	53.8
	1.5	3	42.2	28.4	34.6	23.7	24.2	19.2	34.7	26.2	22.1	18.5	31.9	25.7	17.6	26.6	18.8	26.6	64.1	30.9	49.8	24.9
		5	57.9	39.5	48.0	33.1	33.7	26.9	47.9	36.5	30.8	25.9	44.1	35.7	-35.3	32.0	-33.6	30.2	84.2	42.3	68.1	34.6
		8	81.1	61.1	73.1	52.3	52.7	42.6	70.2	56.2	48.3	41.0	65.7	55.0	-627.9	1.8	-625.1	-18.6	82.5	59.5	93.9	52.9
	2	3	43.7	29.4	33.6	23.2	23.2	18.5	37.1	27.9	21.1	17.8	34.0	27.5	14.5	26.8	19.9	28.7	66.1	32.0	47.5	24.2
		5	59.7	40.8	46.6	32.3	32.3	25.8	51.0	38.6	29.3	24.9	46.7	38.1	-39.9	32.6	-32.3	33.6	85.8	43.6	65.2	33.6
		8	81.8	62.9	71.7	51.2	50.9	41.0	73.7	59.2	46.3	39.5	68.2	58.3	-633.9	5.7	-621.9	-8.2	74.0	59.9	92.2	51.8

Table 9: Calculated dose differences of the $D_{2\%}$ and D_{mean} values if the results of the ^{106}Ru plaque type CCA and the 20 mm ^{125}I COMS plaque are compared. In both simulations the tumor was placed in the anterior position, according to Table 4. The red values are indicating higher ^{106}Ru values.

			lens		optic nerve		macula		retina		ciliary body	
	error		$D_{2\%}$	D_{mean}	$D_{2\%}$	D_{mean}	$D_{2\%}$	D_{mean}	$D_{2\%}$	D_{mean}	$D_{2\%}$	D_{mean}
apex [mm]	0	3	43.8	35.4	16.7	13.6	14.6	12.9	19.6	23.5	13.9	29.0
		5	51.5	47.5	23.4	19.1	20.5	18.1	-20.9	30.8	-26.6	32.4
		8	-11.6	54.9	37.5	30.7	32.8	29.0	-483.1	27.5	-469.9	-25.9

			min		max		min		max		min		max		min		max		min		max	
	error		$D_{2\%}$	D_{mean}	$D_{2\%}$	D_{mean}	$D_{2\%}$	D_{mean}	$D_{2\%}$	D_{mean}	$D_{2\%}$	D_{mean}	$D_{2\%}$	D_{mean}	$D_{2\%}$	D_{mean}	$D_{2\%}$	D_{mean}	$D_{2\%}$	D_{mean}	$D_{2\%}$	D_{mean}
apex height [mm]	0.5	3	37.7	34.9	39.3	33.6	16.1	13.1	17.4	14.2	14.1	12.5	15.2	13.4	30.9	23.2	24.7	24.4	17.4	29.4	17.1	29.2
		5	49.6	48.2	52.8	46.7	22.5	18.4	24.4	19.9	19.7	17.5	21.4	18.7	1.5	30.4	-14.6	31.8	-22.7	32.0	-19.6	33.3
		8	-26.3	53.4	3.1	57.1	36.3	29.7	39.4	32.1	31.8	28.2	34.5	30.2	-379.6	30.3	-473.6	29.2	-467.7	-32.3	-429.6	-16.5
	1	3	43.4	37.2	44.1	34.1	15.6	12.7	18.2	14.8	16.8	12.1	16.1	13.9	38.3	22.9	24.0	24.9	16.8	29.8	20.1	29.4
		5	48.3	49.4	54.5	46.3	22.0	18.0	25.7	20.9	19.4	17.1	22.6	19.6	18.1	30.5	-16.0	32.5	-25.1	32.4	-11.4	34.7
		8	-44.7	50.1	14.6	57.9	35.0	28.5	40.8	33.2	30.8	27.2	35.9	31.2	-309.3	31.3	-494.7	6.7	-499.1	-39.8	-391.6	-8.7
	1.5	3	43.7	32.4	44.7	33.7	15.2	12.4	19.3	15.7	13.4	11.9	17.0	14.7	51.7	22.8	22.3	26.2	19.8	30-7	24.2	30.0
		5	46.4	50.3	55.7	45.7	21.2	17.4	27.1	21.9	18.7	16.7	23.8	20.5	41.8	30.2	-23.9	33.6	-23.0	32.4	-3.5	35.9
		8	-60.8	47.8	26.9	59.5	33.8	27.8	43.1	34.9	39.8	26.6	37.9	32.7	-212.7	32.7	-541.4	25.9	-501.1	-45.3	-347.5	1.0
	2	3	43.4	39.3	44.5	32.9	14.7	12.1	20.5	16.4	12.9	11.6	18.0	15.4	59.0	22.5	17.6	26.8	21.5	31.3	28.8	30.2
		5	44.3	50.9	56.3	44.8	20.5	16.9	28.6	22.9	18.0	16.2	25.2	21.5	57.0	29.9	-33.8	34.2	-22.0	32.5	6.5	36.8
		8	-78.0	44.5	36.1	60.2	32.7	26.9	45.7	36.6	28.7	25.9	40.2	34.3	-139.9	34.2	-585.4	25.4	-508.9	-51.3	-296.4	10.0

Table 10: Calculated dose differences of the $D_{2\%}$ and D_{mean} values if the results of the ^{106}Ru plaque type CCA and the 20 mm ^{125}I COMS plaque are compared. In both simulations the tumor was placed in the posterior position, according to Table 4. The red values are indicating higher ^{106}Ru values.

			lens		optic nerve		macula		retina		ciliary body	
	error		$D_{2\%}$	D_{mean}	$D_{2\%}$	D_{mean}	$D_{2\%}$	D_{mean}	$D_{2\%}$	D_{mean}	$D_{2\%}$	D_{mean}
apex [mm]	0	3	27.6	19.8	38.1	35.2	51.7	41.3	26.2	36.0	34.8	19.7
		5	37.9	27.3	43.2	46.0	64.8	54.1	-27.8	42.1	47.7	27.1
		8	59.7	43.2	-14.6	51.3	45.6	62.5	-621.1	-0.4	74.6	42.8

			min		max		min		max		min		max		min		max		min		max	
	error		$D_{2\%}$	D_{mean}	$D_{2\%}$	D_{mean}	$D_{2\%}$	D_{mean}	$D_{2\%}$	D_{mean}	$D_{2\%}$	D_{mean}	$D_{2\%}$	D_{mean}	$D_{2\%}$	D_{mean}	$D_{2\%}$	D_{mean}	$D_{2\%}$	D_{mean}	$D_{2\%}$	D_{mean}
apex height [mm]	0.5	3	29.1	20.8	34.0	23.4	40.4	34.3	16.0	22.3	49.8	39.8	24.1	24.4	31.0	37.7	30.0	33.7	37.5	20.8	48.2	24.3
		5	39.5	28.3	46.1	31.8	47.9	44.7	12.1	27.8	62.9	52.0	26.2	30.4	-24.2	43.4	-25.6	38.1	50.7	28.3	65.3	33.0
		8	61.9	44.5	72.3	50.0	14.3	53.6	-64.3	22.3	57.9	64.2	-16.0	24.6	-616.4	0.8	-619.7	-7.4	78.5	44.4	101.9	51.9
	1	3	30.6	21.7	34.6	23.8	40.7	33.0	16.7	22.8	47.7	37.8	24.8	25.0	34.3	37.4	33.3	34.7	39.9	21.9	49.1	24.8
		5	41.6	29.5	47.0	32.4	50.4	43.5	13.2	28.6	61.5	49.9	27.3	31.3	-19.0	43.2	-20.4	39.5	54.2	29.7	66.7	33.7
		8	64.2	45.8	72.8	50.3	33.5	54.4	-63.8	22.7	64.8	63.7	-15.4	25.0	-613.8	-1.8	-617.1	-6.6	82.4	45.9	102.6	52.2
	1.5	3	32.2	22.7	35.3	24.3	40.2	32.0	17.5	23.4	45.9	36.3	25.7	25.6	37.4	36.8	37.3	35.8	42.8	23.0	50.2	25.3
		5	43.6	30.8	47.9	33.0	80.8	42.3	14.2	29.3	59.5	48.1	28.3	32.1	-15.4	41.9	-15.8	40.9	57.9	31.2	68.0	34.3
		8	66.7	47.4	73.6	50.8	44.8	54.8	-63.0	23.3	67.9	63.3	-14.6	25.7	-610.9	-6.3	-613.2	-5.5	86.8	47.8	103.7	52.8
	2	3	34.3	24.0	36.5	25.1	40.0	31.4	18.8	24.4	43.8	34.9	27.0	26.7	42.7	38.3	43.4	37.5	46.5	24.6	51.8	26.1
		5	46.0	32.2	49.0	33.8	50.7	41.2	15.3	30.2	56.6	45.9	29.5	33.0	-10.9	43.0	-10.2	42.5	62.1	32.9	69.5	35.1
		8	69.2	48.9	74.2	51.3	51.4	54.4	-62.3	23.8	66.8	61.3	-13.9	26.3	-610.1	-7.8	-609.8	-4.6	91.5	49.6	104.6	53.2

Table 11: Calculated dose differences of the $D_{2\%}$ and D_{mean} values if the results of the ^{106}Ru plaque type CCB and the 20 mm ^{125}I COMS plaque are compared. In both simulations the tumor was placed in the central position, according to Table 4. The red values are indicating higher ^{106}Ru values.

			lens		optic nerve		macula		retina		ciliary body	
	error		$D_{2\%}$	D_{mean}	$D_{2\%}$	D_{mean}	$D_{2\%}$	D_{mean}	$D_{2\%}$	D_{mean}	$D_{2\%}$	D_{mean}
apex [mm]	0	3	27.2	23.2	26.5	21.2	24.4	20.7	9.0	16.0	3.1	17.8
		5	35.5	32.0	36.7	29.6	34.0	28.9	-21.7	16.9	-9.0	22.8
		8	27.1	45.2	52.6	45.5	49.9	44.4	-423.7	-35.2	-165.4	10.3

			min		max		min		max		min		max		min		max		min		max	
	error		$D_{2\%}$	D_{mean}	$D_{2\%}$	D_{mean}	$D_{2\%}$	D_{mean}	$D_{2\%}$	D_{mean}	$D_{2\%}$	D_{mean}	$D_{2\%}$	D_{mean}	$D_{2\%}$	D_{mean}	$D_{2\%}$	D_{mean}	$D_{2\%}$	D_{mean}	$D_{2\%}$	D_{mean}
apex height [mm]	0.5	3	27.1	23.6	27.7	22.9	25.3	20.4	27.9	22.3	23.1	19.7	25.5	21.7	10.1	17.1	9.8	16.4	-5.0	17.2	9.0	18.5
		5	34.9	32.5	36.6	31.6	35.0	28.4	38.4	31.1	32.0	27.5	35.2	30.2	-20.8	18.6	-21.3	17.3	-23.3	21.3	1.1	23.9
		8	21.9	45.2	34.3	45.9	51.5	44.4	54.4	47.5	48.0	43.0	50.8	46.3	-418.4	-28.6	-421.1	-34.8	-217.7	3.4	-125.1	16.8
	1	3	27.4	24.1	27.6	22.6	24.3	19.6	29.4	23.5	22.2	19.0	27.6	23.0	11.3	17.8	10.4	16.5	-7.7	16.6	13.8	18.9
		5	35.3	33.3	37.1	31.4	34.0	27.5	40.5	32.8	31.1	26.7	38.3	32.2	-17.8	20.1	-19.3	17.4	-28.2	20.3	10.1	25.1
		8	17.3	44.2	36.7	45.6	50.3	42.6	54.5	48.8	46.5	41.4	53.8	47.8	-418.9	-25.0	-423.4	-39.4	-246.8	-4.5	-91.5	21.4
	1.5	3	27.5	24.9	27.6	22.4	23.5	19.0	31.3	25.0	21.4	18.3	29.5	24.5	12.5	17.7	12.6	15.7	-13.0	16.2	18.6	19.5
		5	34.4	33.8	36.9	31.1	32.6	26.5	42.7	34.6	29.8	25.5	40.4	33.8	-17.9	19.8	-18.0	15.5	-38.9	18.8	17.9	25.9
		8	10.4	43.8	39.1	45.9	49.5	41.5	55.6	51.0	45.4	40.0	55.4	49.7	-417.6	-23.0	-420.6	-46.6	-290.4	-12.2	-59.9	26.2
	2	3	26.8	25.3	27.6	22.1	22.7	18.3	33.0	26.4	20.7	17.6	31.0	26.0	9.4	17.7	13.1	15.0	-16.6	15.4	21.8	19.7
		5	32.7	34.2	36.9	30.6	31.5	25.5	44.6	36.4	28.7	24.6	42.2	35.9	-22.4	19.8	-17.8	14.1	-46.0	17.1	23.8	26.3
		8	0.8	42.7	42.1	45.9	48.5	40.3	55.8	52.9	44.5	38.8	55.8	51.9	-423.6	-21.8	-420.8	-52.6	-323.0	-20.7	-34.7	29.5

Table 12: Calculated dose differences of the $D_{2\%}$ and D_{mean} values if the results of the ^{106}Ru plaque type CCB and the 20 mm ^{125}I COMS plaque are compared. In both simulations the tumor was placed in the anterior position, according to Table 4. The red values are indicating higher ^{106}Ru values.

			lens		optic nerve		macula		retina		ciliary body	
	error		$D_{2\%}$	D_{mean}	$D_{2\%}$	D_{mean}	$D_{2\%}$	D_{mean}	$D_{2\%}$	D_{mean}	$D_{2\%}$	D_{mean}
apex [mm]	0	3	11.5	23.9	16.6	13.6	14.5	12.9	-16.1	16.2	-9.7	11.6
		5	3.6	29.9	23.4	19.1	20.4	18.1	-56.4	19.9	-43.3	8.1
		8	-136.3	5.6	37.3	30.6	32.6	29.0	-417.8	-0.5	-405.6	-81.1

			min		max		min		max		min		max		min		max		min		max	
	error		$D_{2\%}$	D_{mean}	$D_{2\%}$	D_{mean}	$D_{2\%}$	D_{mean}	$D_{2\%}$	D_{mean}	$D_{2\%}$	D_{mean}	$D_{2\%}$	D_{mean}	$D_{2\%}$	D_{mean}	$D_{2\%}$	D_{mean}	$D_{2\%}$	D_{mean}	$D_{2\%}$	D_{mean}
apex height [mm]	0.5	3	10.1	23.8	12.2	24.3	16.0	13.1	17.4	14.2	14.0	12.5	15.2	13.4	-21.1	16.5	-10.2	17.3	-4.7	13.1	-12.9	11.6
		5	0.4	29.2	5.2	30.6	22.5	18.4	24.4	19.9	19.7	17.5	21.3	18.7	-63.7	20.5	-48.7	21.3	-36.9	8.5	-48.3	8.1
		8	-151.8	0.3	-124.0	11.8	36.2	29.7	39.2	32.1	31.6	28.2	34.2	30.2	-479.6	4.2	-457.1	2.2	-394.0	-83.2	-410.6	-76.5
	1	3	8.3	23.7	12.6	24.6	15.6	12.7	18.1	14.8	13.7	12.1	16.0	13.9	-26.0	16.6	-7.5	17.2	0.5	13.1	-16.6	11.4
		5	-2.7	28.9	6.8	31.8	22.0	17.9	25.5	20.9	19.4	17.1	22.5	19.6	-69.6	21.0	-43.7	21.2	-28.6	9.6	-52.4	8.5
		8	-171.8	-6.8	-115.9	16.5	34.9	28.5	40.3	33.1	30.7	27.1	35.6	31.1	-492.9	6.2	-454.1	-1.9	-385.4	-86.4	-419.2	-73.6
	1.5	3	8.7	24.0	16.2	25.2	15.1	12.4	19.2	15.6	13.4	11.9	16.9	14.6	-26.6	16.6	-0.6	18.1	5.2	14.1	-19.1	11.8
		5	-3.8	28.4	12.5	32.6	21.2	17.4	26.9	21.8	18.7	16.7	23.6	20.5	-71.6	21.0	-35.8	21.9	-23.5	10.3	-56.9	9.0
		8	-181.8	-12.3	-92.0	22.0	33.7	27.7	42.5	34.8	29.7	26.6	37.3	32.5	-493.1	8.0	-441.7	-3.3	-376.2	-88.4	-422.1	-68.2
	2	3	9.0	23.9	18.3	25.4	14.7	12.1	20.3	16.4	12.8	11.6	17.9	15.3	-30.9	16.7	1.9	18.6	9.6	14.9	-21.7	11.8
		5	-4.2	27.7	16.2	33.0	20.5	16.9	28.3	22.8	17.9	16.2	24.9	21.4	-77.7	21.2	-32.6	22.3	-17.6	11.0	-60.3	9.4
		8	-189.8	-18.5	-75.1	26.4	32.7	27.0	44.8	36.4	28.6	25.9	39.4	34.0	-500.3	10.6	-436.8	-4.3	-366.0	-90.0	-422.7	-63.0

Table 13: Calculated dose differences of the $D_{2\%}$ and D_{mean} values if the results of the ^{106}Ru plaque type CCB and the 20 mm ^{125}I COMS plaque are compared. In both simulations the tumor was placed in the posterior position, according to Table 4. The red values are indicating higher ^{106}Ru values.

			lens		optic nerve		macula		retina		ciliary body	
	error		$D_{2\%}$	D_{mean}	$D_{2\%}$	D_{mean}	$D_{2\%}$	D_{mean}	$D_{2\%}$	D_{mean}	$D_{2\%}$	D_{mean}
apex [mm]	0	3	26.4	19.7	23.9	32.0	53.9	34.7	19.3	15.5	29.3	18.8
		5	36.0	27.0	23.9	41.8	71.0	44.6	-13.2	11.7	38.9	25.6
		8	53.9	42.2	-53.0	44.0	80.5	38.6	-419.2	-77.8	47.1	38.0

			min		max		min		max		min		max		min		max		min		max	
	error		$D_{2\%}$	D_{mean}	$D_{2\%}$	D_{mean}	$D_{2\%}$	D_{mean}	$D_{2\%}$	D_{mean}	$D_{2\%}$	D_{mean}	$D_{2\%}$	D_{mean}	$D_{2\%}$	D_{mean}	$D_{2\%}$	D_{mean}	$D_{2\%}$	D_{mean}	$D_{2\%}$	D_{mean}
apex height [mm]	0.5	3	27.7	20.6	32.8	23.2	31.6	31.9	1.8	19.2	36.2	35.2	0.1	17.9	23.7	17.8	23.1	13.2	31.0	19.7	42.7	23.4
		5	37.2	27.9	44.2	31.5	36.2	41.4	-7.2	23.6	42.6	45.3	-10.3	20.8	-10.3	14.1	-11.1	7.7	40.3	26.4	556.	31.5
		8	54.8	43.3	66.5	49.1	-5.8	48.0	-102.6	15.0	5.2	48.0	-115.2	0.7	-416.5	-73.1	-417.8	-84.7	46.1	38.6	74.4	47.1
	1	3	28.8	21.4	33.4	23.6	33.8	31.1	2.5	19.7	38.3	34.3	0.9	18.4	27.3	19.2	26.4	14.2	32.1	20.5	43.6	23.8
		5	38.7	29.1	45.2	32.1	41.1	40.9	-6.2	24.5	47.5	44.9	-9.2	21.7	-4.7	16.6	-5.9	9.2	41.4	27.5	57.9	32.2
		8	55.4	44.4	67.0	49.4	16.4	49.8	-102.1	15.4	29.2	51.5	-114.6	1.2	-412.7	-67.1	-415.2	-84.0	42.7	38.9	75.1	47.5
	1.5	3	30.0	22.3	34.2	24.2	34.9	30.4	3.3	20.3	39.7	33.6	1.7	19.1	30.7	21.1	30.3	15.3	33.4	21.4	44.7	24.4
		5	40.2	30.2	46.0	32.7	43.7	40.1	-5.2	25.2	50.7	44.2	-8.2	22.5	-0.7	19.6	-1.3	10.5	42.6	28.5	59.1	32.8
		8	55.9	45.6	67.8	49.9	31.1	50.6	-101.3	16.0	46.2	53.8	-113.8	1.8	-408.6	-57.7	-411.3	-82.9	39.4	39.4	76.1	48.0
	2	3	31.6	23.6	35.3	25.0	35.5	30.0	4.6	21.2	39.1	32.8	3.0	20.1	36.2	23.2	36.4	17.0	35.3	22.5	46.3	25.2
		5	41.7	31.5	47.1	33.5	44.6	39.4	-4.0	26.1	49.8	42.9	-7.0	23.5	4.2	21.6	4.3	12.1	44.0	29.7	60.6	33.6
		8	56.1	46.7	68.4	50.4	39.1	50.9	-100.6	16.5	50.6	53.9	-113.0	2.4	-406.4	-55.7	-407.9	-81.9	35.4	39.6	77.0	48.5

4. Discussion

4.1. Monte Carlo generated dose libraries

The implementation of the 24 individual npz-files, each representing the dose lookup table of one single radioactive seed and the 24 toggle boxes representing these seeds, enable the simulation of individual treatment methods according to the treatment plan and the loading diagram. Comparing this method with one of the ^{106}Ru plaque types CCA or CCB, for which the radioactive layer is fixed, using the 20 mm ^{125}I COMS plaque provides the opportunity to vary the orientation of the radiation field by ticking the seeds on demand.

The implementation of the dose lookup tables and the geometrical shape of the plaques form the basis for the treatment planning system and the dose calculation.

4.2. Adapting the treatment planning systems for ^{125}I COMS plaques

As previously stated in section 2.2.2 a new global parameter for the eye radius was implemented, which made it possible to change its value manually according to the required simulation. This very efficient implementation is limited by the fact that for the new implemented 20 mm ^{125}I COMS plaque, not only the eye radius differed to the one of the simulations with one of the ^{106}Ru plaque types CCA or CCB, also the position of the tumor was adjusted. As described in section 2.2.2 its distance to the xy – surface was shortened. Unlike the other OARs that were linked to the new global eye parameter and whose parameter were changed simultaneously according to the typed in value, the distance parameter of the tumor couldn't be linked to it in this model. This had still to be changed separately. This way this simulated eye model is not as variable and flexible as originally intended. If the plaque type is changed during treatment planning from one of the ^{106}Ru plaques to the 20 mm ^{125}I COMS plaque, the eye radius has to be changed additionally.

4.3. Dosimetric considerations of ^{125}I COMS plaques

4.3.1. Tumor Coverage

As already mentioned in section 3.2.1 the maximum basal diameter of a tumor, which still can be effectively irradiated is almost linearly dependent on its apex height. Hence, the possible coverable basal diameter was increasing with an increasing apex height. Smaller apex heights resulted in smaller basal diameters, since the resident time to get a prescribed dose of 85 Gy at the apex was shorter for smaller tumors, resulting in a smaller, lateral dose deposition.

The investigation of the tumor coverage of Plaque1 revealed that tumors of the neutral position with an apex height of 8 mm and a maximum basal diameter of 16 mm were the largest that were able to be covered with the 20 mm ^{125}I COMS plaque. A previous study by Heilemann *et al.* [34] showed that using the ^{106}Ru plaque type CCB for the treatment of a tumor in the same position enabled to cover a tumor of an apex height of 8 mm and a basal diameter of 19 mm. The difference of 3 mm can be explained by the fact that the radioactive layer of the ^{106}Ru plaques is covering the whole surface of the plaque stretching almost to the edges, whereas, the outer ring of the radioactive seeds of the 20 mm ^{125}I COMS plaque is not directly placed at the edge of the plaque, but a few millimeters are spared, as can be seen in Figure 9. Consequently, Plaque2, where the grooves 1 to 9 were not occupied, resulted in a smaller maximum coverable basal diameter of 14 mm for an apex height of 8 mm.

Additionally, to the neutral position the displacement of 1 mm and 2 mm was investigated too. With an increasing displacement the larger tumors were not entirely covered by the plaque anymore resulting in smaller maximum basal diameters of a tumor whose V95 values equal 100%, because the peripherical regions of the tumor did not receive enough dose anymore. The maximum basal diameter of Plaque1 was decreasing to 13 mm for 1 mm displacement and to 11 mm for 2 mm displacement. By shifting Plaque2 1 and 2 mm from the neutral position it was possible to cover a tumor with a basal diameter of 13 mm and 10 mm, respectively. Although the displacement resulted in smaller, coverable tumor basal diameters, it can be useful in sparing OARs.

The comparison of the results for the maximum coverable basal diameter of the 20 mm ^{125}I COMS plaque with the ones of the study of the ^{106}Ru plaque types CCA and CCB investigated by Heilemann *et al.* [34], for the neutral position as well as the displacement positions showed that it is not possible to cover as large tumors with the 20 mm ^{125}I COMS plaque as with the ^{106}Ru plaque types.

On the basis of Figure 19 and Figure 20, that both illustrate the tumor coverage as a function of the tumor basal diameter and its apex height, it can be seen that the dose gradient of Plaque1 and Plaque2 is not as steep as it was discovered for the ^{106}Ru plaque types CCA and CCB by Fetty [1]. Due to their longer range, the ^{125}I photons can penetrate further into the tissue, whereas the ^{106}Ru electrons deposit their energy in the closer vicinity.

Additionally, it can be seen that the 20 mm ^{125}I COMS plaque is more stable with regard to the displacement of the plaque relative to the tumor. Since the plaque is not always placed perfectly in the required position on the eye during a surgery, but can be displaced a bit, this phenomenon might be of a great advantage. Due to the stability the risk of deviations between the absorbed dose values, that occur due to displacements, might not be as high as for the ^{106}Ru plaque types.

Table 14 - Table 19 list the resulting $D_{98\%}$ values in Gray for Plaque1 and Plaque2. Taking a look at them it can be seen, that for a fixed basal diameter the $D_{98\%}$ values were increasing with increasing apex height, based on longer treatment times that were necessary to get a

prescribed dose of 85 Gy at the apex. Consequently, more photons were penetrating into the tumor tissue and were transferring their energy to it. Conversely, for a fixed apex height and increasing basal diameters the $D_{98\%}$ values were decreasing. By the time the apex receives the required dose of 85 Gy, the dose distribution to the peripheral regions of the tumor is too low, based on the conical forward directed radiation field.

4.3.2. Organs at risk

The investigations of the absorbed dose by the OAR showed an increase with a decreasing distance of the plaque to the OAR, with the only exception of the optic nerve when the tumor was placed in the posterior region of the eye. Furthermore, it can be said that the absorbed dose was increasing too with an increasing apex height of the tumor. This is based on the longer treatment times that were needed for larger tumors. As a consequence more particles were emitted by the plaques and thereby the dose distributed to the tissue increased.

To get an overview of which tumor configuration would be preferably treated with one of the ^{106}Ru plaque types CCA or CCB and with the 20 mm ^{125}I COMS plaque, first of all the graphs (a) to (e) of Figure 21 were compared to the ones of the simulations with ^{106}Ru pictured in the publication [34] by Heilemann *et al.*. In a second step the resulting $D_{2\%}$ and D_{mean} values of the simulation with ^{106}Ru plaque types CCA and CCB were subtracted from the one with the 20 mm ^{125}I COMS plaque, to see whether the OARs absorbed more dose treating the tumor with one of the ^{106}Ru plaque types CCA or CCB, or the 20 mm ^{125}I COMS plaque. These results are listed in Table 8 to Table 13.

Absorbed near maximum dose values $D_{2\%}$ of the lens for an anterior placed tumor

Comparing the $D_{2\%}$ values of the lens for an anterior positioned tumor resulting from the simulation with the 20 mm ^{125}I COMS plaque, illustrated in graph (a) of Figure 21, and the one of the simulations with the ^{106}Ru plaque types by Heilemann *et al.* [34], it can be seen that the course of the curves of ^{106}Ru look similar to the one of ^{125}I. Both of them show a decreasing behavior with an increasing distance to the lens. For smaller apex heights (3 mm and 5 mm) a treatment with the 20 mm ^{125}I COMS plaque resulted in higher values than using either the CCA or CCB ^{106}Ru plaque type. This bases on the longer range of the photons inside a tissue, which enables them to transfer their energy to the more distant parts. The opposite effect was observed for tumors with an apex height of 8 mm. In this scenario the lens absorbed more dose if one of the ^{106}Ru plaque types was used. It seemed as if in this case based on the longer treatment time, which was necessary to get the prescribed dose of 120 Gy at the apex, thus the larger number of high energetic low-ranged electrons that were emitted had a more significant effect than the long-ranged photons.

Absorbed near maximum dose values $D_{2\%}$ of the optic nerve and the macula for an anterior placed tumor

Additionally, the $D_{2\%}$ values of the optic nerve and the macula were calculated for an anterior located tumor. As can be seen in graph (a) of Figure 21 and by comparing the calculated values with the ones of the simulations with the ^{106}Ru plaque types CCA and CCB in the publication [34] by Heilemann *et al.*, it can be seen that although the plaque is placed on the opposite side of the optic nerve, both OAR still absorbed enough dose that might result in some severe damage. While the optic nerve as well as the macula didn't even absorb 1 Gy using a CCA or CCB ^{106}Ru plaque, applying the 20 mm ^{125}I COMS plaque, the macula absorbed 15 Gy, 20 Gy and 33 Gy and the optic nerve 17 Gy, 23 Gy and 38 Gy for tumor with ascending apex height (3, 5 and 8 mm). These high values compared to the ones of the previous ^{106}Ru by Heilemann e*t al.* [2] can be traced back to the fact that the photons can penetrate further into the tissue and thereby transfer their energy to more distant parts.

Absorbed near maximum dose values $D_{2\%}$ of the lens and the optic nerve for a central placed tumor

As can be seen in graph (b) of Figure 21, for a central positioned tumor the absorbed near maximum dose values of the lens showed a similar behavior as for the anterior located tumor with the sole difference that the absorbed $D_{2\%}$ dose values were generally lower. The optic nerve showed the reverse effect. Its absorbed $D_{2\%}$ dose values were increasing with a decreasing movement of the plaque towards the optic nerve. The comparison of the resulting absorbed dose values of both OARs, for a centrally placed tumor and a neutrally placed plaque, of the ^{125}I COMS plaque study with the preceding ^{106}Ru study by Heilemann *et al.* [2] yielded larger values for the 20 mm ^{125}I COMS plaque. This phenomenon again bases on the physicals property of the photons also transferring their energy to more distant parts.

Absorbed near maximum dose values $D_{2\%}$ of the optic nerve and the macula

The OARs that were mostly affected by the posterior placement of the tumor, were the macula and the optic nerve. The simulations that were carried out therefore, show that independently of the apex height of the tumor the $D_{2\%}$ of both OARs showed a maximum for the neutral position of the plaque and a decreasing behavior by shifting it away from the optic nerve. For a movement towards the optic nerve both OAR showed a different behavior than expected. Instead of remaining constant, as it was observed for the ^{106}Ru plaque types CCA and CCB within the study published by Heilemann *et al.* [34], their $D_{2\%}$ values firstly dropped down till the plaque was shifted +0.5 mm and were afterwards slightly increasing again. We assumed that this could be explained by a combination of a few reasons. First, the ^{106}Ru plaques were already contacting the optic nerve in the neutral plaque position and were overlapping with the optic nerve by shifting the plaque closer to it. However, this seemed not to be the case for the 20 mm ^{125} COMS plaque. The reason therefore could be the straight edges causing a cylindrical shape whereby it is not stretching towards the optic nerve. Next,

for the neutral position of the plaque we assumed that the photons that were emitted on the side of the plaque facing the optic nerve, were still directed towards the OARs. Shifting the plaque closer to the optic nerve it looked like that these photons were not directed towards the optic nerve and the macula anymore. The ones which would be directed to the OARs were shielded by the gold-alloy backing on the convex side of the plaque, which is depicted in Figure 22.

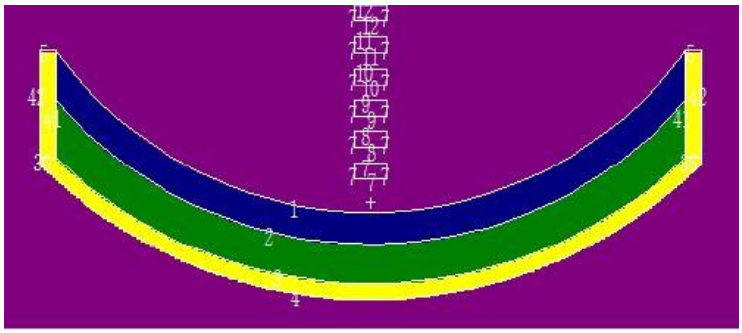

Figure 22:Illustration of the plaque geometry showing the silastic seed carrier (green), a pure silastic carrier without any grooves for seeds (blue) and the gold-alloy backing (yellow) (from[35]*).*

Apart from that some other interesting differences for the optic nerve and the macula were observed. Comparing the results of the CCA ^{106}Ru plaque with the ones of the 20 mm ^{125}I COMS plaque, it was shown that both OAR absorbed more dose by using the 20 mm ^{125}I COMS plaque for treating tumors with an apex height of 3 and 5 mm. If a tumor with an apex height of 8 mm was treated this only applied for the central and anterior position of the tumor. If the tumor was located posterior this changed by moving the plaque closer to the optic nerve. In this case the optic nerve as well as the macula absorbed more dose if a tumor with an apex height of 8 mm was treated with a CCA ^{106}Ru plaque.

A similar behavior was observed for the comparison of the 20 mm ^{125}I COMS plaque with the CCB ^{106}Ru plaque. For the anterior as well as for the central tumor position the absorbed $D_{2\%}$ values by the optic nerve and the macula, using the 20 mm ^{125}I COMS plaque were again higher. If the tumor was placed on the back side of the eye and the plaque was shifted closer to the optic nerve, the absorbed $D_{2\%}$ values of both OARs, resulting by a treatment of tumors with an apex height of 5 and 8 mm, were higher using a CCB plaque. It seemed as if a posterior tumor of an apex height of 8 mm was treated, based on the longer resident time and thus increasing number of high energetic electrons, they had a more significant effect on the optic nerve and the macula, than the long-ranged photons.

Absorbed near maximum dose values $D_{2\%}$ of the lens for a posterior placed tumor

In addition to the macula and the optic nerve also the $D_{2\%}$ values of the lens were analyzed for the posterior position of the tumor, as can be seen in graph (c) of Figure 21. The curve shape is inversely to the one of the macula and the optic nerve. The $D_{2\%}$ values as usual were decreasing by moving the plaque from -2 mm to the neutral position, resulting in a minimum. Shifting it further towards the optic nerve the values were firstly increasing strongly till +0.5 mm and were then only slightly increasing by further moving the plaque towards the optic nerve. We assumed that, by shifting the plaque 0.5 mm closer to the optic nerve, due to the forward directed conical radiation field and the shielding effect on the convex side of the plaque, based on the gold-alloy backing, the photons were emitted under an angle that directed them towards the lens. According to their long range inside a tissue they transferred their energy to this distant part, resulting in near maximum values of 28 Gy, 38 Gy and 60 Gy for tumors with an apex height of 3, 5 and 8 mm, respectively. Whereas if a CCA plaque was used the lens did not even absorb 1 Gy. If a CCB plaque was applied the absorbed dose values for irradiating a tumors with an apex height of 3 or 5 mm were below 2 Gy and for and apex height of 8 mm it did not exceed 6 Gy. A previous publication by Groenewald *et al.* [38] mentioned that, if a lens receives more than 8-10 Gy the probability of the occurrence of cataract increases. Comparing this threshold value with the $D_{2\%}$ values the lens absorbed within the ^{125}I COMS study by an opposite placement of the plaque, we can see that due to the long range of the photons this can lead to severe damage of the OAR.

Averaged absorbed dose values D_{mean} and absorbed near maximum values $D_{2\%}$ of the retina

For the retina the D_{mean} values were observed and plotted in graph (d) of Figure 21. However, since also a punctual high radiation exposure of the retina can result in some damage, such as a retinopathy, that can further imply some severe damage, also the $D_{2\%}$ values were of interest and investigated for the central position of the tumor, and plotted in graph (e) of Figure 21. The higher absorbed D_{mean} as well as the $D_{2\%}$ values by the retina for the increasing tumor apex height can again be explained by the longer treatment time and thus increasing number of the emitted photons that are transferring their energy to the tissue of the OAR. The absorbed dose showed a slightly increase for a movement towards the optic nerve, which originates from the fact that the retina does not stretch out until the lens. This results in a smaller average volume that is irradiated if the plaque is moved towards the lens, whereas the irradiated volume is increasing with decreasing distance to the optic nerve, thus resulting in higher dose values. This applies as much to the D_{mean} values as to the $D_{2\%}$ values.

As already expected, according to the longer range of the photons within a tissue, compared to the electrons, the investigation of the retina for the central position, depicted in graph (d) of Figure 21, showed higher absorbed D_{mean} values for treating tumors with an apex height of 3 and 5 mm using the 20 mm ^{125}I COMS plaque. The opposite effect showed tumors with an apex height of 8 mm. For this tumor configuration it seemed as if the increasing

number of high energetic electrons with the increasing treatment time were distributing more energy to the tissue compared to the photons, although they have a shorter range.

Additionally, to the averaged absorbed dose by the retina also the near maximum dose $D_{2\%}$ was observed and compared to the results of the ^{106}Ru study by Heilemann *et al.* [2]. As already expected the absorbed dose values of the retina, with a few exceptions especially for tumors of an apex height of 3 mm, as can be seen in Table 8 to Table 13, were almost always higher using a ^{106}Ru plaque type. Based on the close distance between the plaque surface and the retina the short ranged high energetic electrons were more effective than the large ranged low energetic photons. Furthermore, another positive aspect using the 20 mm ^{125}I COMS plaque was observed by taking a look at the $D_{2\%}$ values plotted in graph (e) of Figure 21. Comparing these values to the threshold value of 500 Gy to the retina, which was stated as a possible predictor in visual acuity loss in a previous publication by Heilemann *et al.* [39], it can be seen that this value will by far be not exceeded. With none of the simulated scenarios, whether for an anterior, a central nor a posterior placed tumor. The results of these observed scenarios clearly demonstrated that the 20 mm ^{125}I COMS plaque is superior to the ^{106}Ru plaque types in sparing the retina.

Absorbed near maximum dose values $D_{2\%}$ of the ciliary body

Results of the observations that were not illustrated in the graphs (a) to (e) of Figure 21, but can be seen in Table 8 to Table 13, providing the calculated dose differences between the CCA and the 20 mm ^{125}I COMS plaque and the CCB and the 20 mm ^{125}I COMS plaque, are the following.

If a posterior position tumor is treated the ciliary body absorbed more dose using the 20 mm ^{125}I COMS plaque, which again based on the longer range of the photons compared to the one of the electrons. For an anterior positioned tumor, the $D_{2\%}$ values of the ciliary body were almost always higher using a CCB plaque, whereas using a CCA plaque this only held true for treating tumors with an apex height of 5 and 8 mm. For a central placement of the tumor, the resulting absorbed dose values of the ciliary body were always higher using the CCB plaque and not the 20 mm ^{125}I COMS plaque, if the plaque was shifted towards the lens. If it was shifted to the other side the values dropped below the ones of the 20 mm ^{125}I COMS plaque for tumors with an apex height of 3 and 5 mm. Comparing the absorbed $D_{2\%}$ values of the ciliary body if a CCA plaque is applied to treat a tumor in a central position to the ones resulting from a treatment with the 20 mm ^{125}I COMS plaque, it can be seen that the values applying the latter one were always higher for all tumor configurations. The difference of the results for a central placed tumor between the CCA and the CCB plaques might be explained by the fact that the CCB plaque is larger in diameter and thereby the distance to the ciliary body decreased. This way it seemed as if the short-ranged electrons were more effective compared to the photons. Using a CCA plaque it seemed as if the long-ranged photons were more effective, based on the increasing distance between the CCA plaque and the ciliary body.

As mentioned in section 2.2.2 the eye radius differed between the simulated models of the 20 mm ^{125}I COMS plaque and the ^{106}Ru ones. The differences of the angles between the middle line of the optic nerve and the one of the tumor that arise from the 0.3 mm deviation of the eye radius were different for the various tumor positions. The one for the posterior location was 0.6°, the one for the central position 1.4° and the one for the anterior placement 2.2°. As a result, if an anterior placed tumor is irradiated, the absorbed dose values the OARs show for a neutral plaque position of the ^{106}Ru plaque types correspond to the ones of the ^{125}I COMS plaque which is shifted about 0.5 mm. If the tumor is located in the center the absorbed dose values of the OARs for a neutrally positioned ^{106}Ru plaque are correlated to the ones they show for a ^{125}I COMS plaque which is moved about 0.3 mm. For a posterior placed tumor the absorbed dose values of the individual OARs by a neutrally placed ^{106}Ru plaque correspond to the ones resulting of the irradiation of the same tumor with a ^{125}COMS plaque shifted about 0.1 mm. Based on the high differences between the absorbed dose values resulting from the different treatment modalities, the 20 mm ^{125}I COMS plaque and one of the ^{106}Ru eye plaques, these small deviations of the angles and thereby shifted position values, do not have a strong influence on the results, but have to be kept in mind.

Possible approach to decision making to find out which treatment modality would be most efficient

According to the above discussed results it can be seen that the physicians always have to individually decide whether a treatment applying the 20 mm ^{125}I COMS plaque or one of the ^{106}Ru eye plaque would be most efficient. The first aspect they have to consider would be the tumor coverage. The study that was carried out in course of this master thesis brought up that the tumor coverage using the 20 mm ^{125}I COMS plaque was superior to the one of the ^{106}Ru plaques with regard to plaque displacements. But if the tumor basal diameter exceeds a certain value the 20 mm ^{125}I COMS cannot be used anymore. In a next step it has to be taken account of whether the retina should be spared, but thereby higher absorbed dose values of the OARs, especially the ones that are placed at more distant parts or even opposite the plaque, can be risked. As can be seen the decision depends on a few factors, such as the apex height, the tumor position inside the eye and which OARs especially have to be spared.

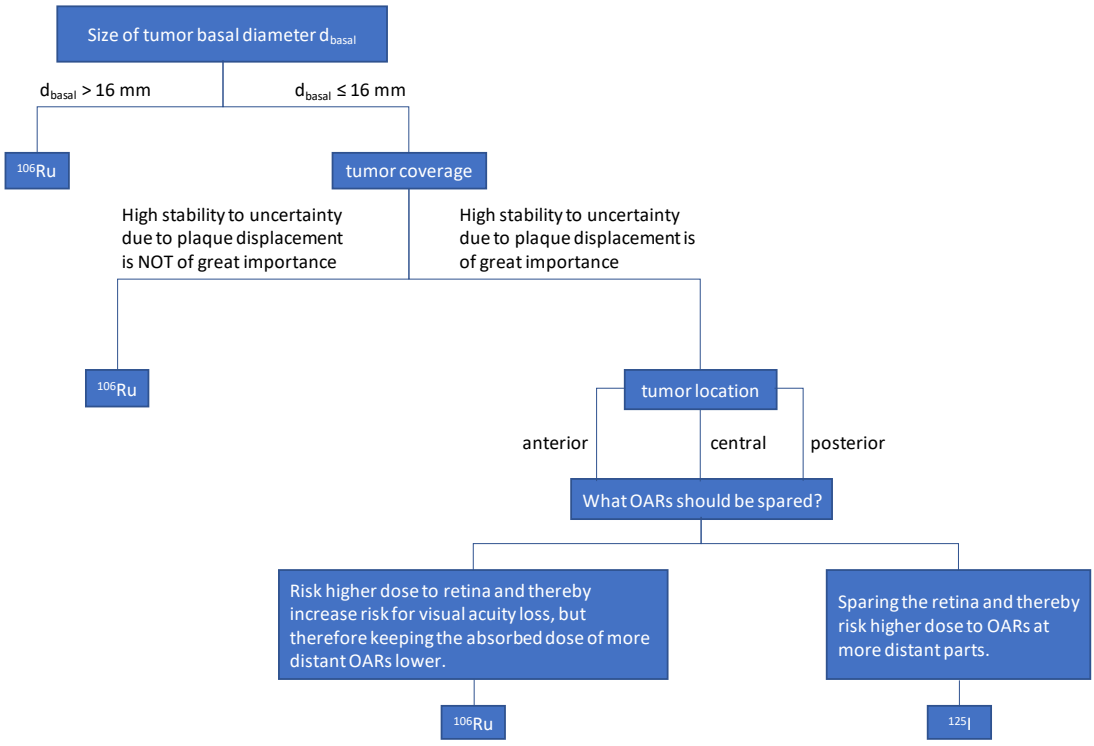

Figure 23: Possible decision support for the treatment of uveal melanoma using either ^{125}I or ^{106}Ru eye plaque brachytherapy

5. Conclusion

The simulations of the different tumor configurations, their positions inside the eye and the different placements of the 20 mm ^{125}I COMS plaque and the comparison of these results with the ones of the preceding study with the ^{106}Ru plaque types CCA and CCB by Heilemann *et al.*[34] showed that it is not possible to make a general statement, whether one of the ^{106}Ru plaque types or the 20 mm ^{125}I COMS plaque is more efficient in treating a certain tumor configuration.

The tumor coverage study demonstrated that the efficiency of treating a tumor is decreasing with an increasing apex height and basal diameter. Furthermore, if the basal diameter reaches a certain value, these tumors cannot be treated with the 20 mm ^{125}I COMS plaque anymore, whether within plaque configuration Plaque1 nor Plaque2. Tumors with larger basal diameters than that should be treated with a larger sized ^{125}I COMS plaque or a similar sized ^{106}Ru plaque. Although the coverable diameters are smaller than for the ^{106}Ru plaque types the ^{125}I COMS plaque study showed better results with regards to the dose gradient, which was smoother and more stable in between the displacement positions, making it less prone to small application errors during surgery.

As already discussed in section 3.2.2 and as it was expected based on the different physical properties of electrons and photons, the near maximum dose $D_{2\%}$ in the retina was in most of the cases higher using either the CCA or CCB ^{106}Ru plaque type. Thus, the 20 mm ^{125}I COMS is more efficient in sparing the retina. Therefore, it was shown that the risk of visual acuity loss with respect to the findings from Heilemann *et al.* [39] using the 20 mm ^{125}I COMS plaque is not as high as the one for the ^{106}Ru plaque types.

The study of the OARs showed that there are many factors that have to be kept in mind, which make it more difficult to get to a final conclusion. As a general rule, if the tumor was smaller in its apex height the OARs received less dose. Additionally, the result of this master project pointed out that in most cases displacing the plaque away of the OARs enabled sparing them. On the contrary it still has to be kept in mind, that even if one OAR is placed on the opposite to the 20 mm ^{125}I COMS plaque, it might absorb enough dose causing some severe damage to it.

Furthermore, this investigation revealed that, using a 20 mm ^{125}I COMS plaque to treat a posterior positioned tumor would result in a better sparing of the optic nerve by moving the plaque towards it, compared to the usage of a ^{106}Ru plaque type. If there would be an ^{125}I COMS plaque type be existing that includes a notch for the optic nerve, such as the COB plaque type of the ^{106}Ru ones, we assumed that this might be a good alternative to treat tumors in

the posterior region. This way the optic nerve could be spared even better, especially if the plaque has to be shifted even closer to the optic nerve.

Treating patients with uveal melanoma physicians always have to keep both concepts in mind, the tumor coverage and the OAR exposure. Although the systematic comparison of both studies, the one of the ^{106}Ru plaque types CCA and CCB by Heilemann *et.al* [34] to the one of the 20 mm ^{125}I COMS plaque in framework of this master thesis, showed significantly better results concerning the tumor coverage and sparing the retina, in most of the cases the OARs absorbed more dose if the tumor is treated with the 20 mm ^{125}I COMS plaque. Therefore, it is not possible to provide a general rule for the optimal plaque selection, but this comparison study might be helpful for the physicians to orientate themselves and decide which treatment method would be most efficient.

Future Work

The results showed that the tumor coverage of the 20 mm ^{125}I COMS plaque is more stable with regards to plaque displacements, but limited to smaller coverable maximum basal diameters. Thus, in future work, based on the already existing architecture of the 20 mm ^{125}I COMS plaque inside the 3D animation software Houdini FX (Side Effects Software Inc., Toronto, Canada), the next larger one of 22 mm could be implemented too, to compare if even larger tumors than with the ^{106}Ru plaque types could be efficiently covered with this one. Furthermore, maybe some other isotopes e.g. ^{90}Y could be implemented too for additional comparisons.

Hence, only the tumor coverage of the two different plaque configurations Plaque1 and Plaque2 and the absorbed dose of the OAR for Plaque1 were investigated in this study, some other configurations and even more specific ones, e.g. one where only the grooves of one side of the plaque are occupied and the other side of it is empty, could be investigated too. In addition, also other shapes of tumors such as mushroom-shaped ones could be observed too.

It might also be of interest to modify the restriction due to the distance of the tumor, that is not adjusting automatically according to the typed in value of the eye radius, but has to be changed separately, to be even more flexible with the simulation of different cases.

6. References

[1] L. Fetty, “3D dosimetry for brachytherapy of uveal melanoma,” Fachhochschule Wiener Neustadt, 2017.

[2] G. Heilemann *et al.*, “Treatment plan optimization and robustness of 106 Ru eye plaque brachytherapy using a novel software tool,” *Radiother. Oncol.*, vol. 123, no. 1, pp. 119–124, Apr. 2017.

[3] D. Baltas, L. Sakelliou, and N. Zamboglou, “Radiation Quantities and Units,” in *The Physics of Modern Brachytherapy for Oncology*, 1st ed., Boca Raton, FL: Taylor & Francis Group, 2007.

[4] Z. Li, “Radiobiology of Low- and High-Dose-Rate Brachytherapy,” in *Technical Basis of Radiation Therapy*, 4th ed., S. Levitt, J. Purdy, and C. Perez et al., Eds. Berlin Heidelberg, Germany: Springer, 2006.

[5] N. Suntharalingam, E. B. Podgorsak, and H. Tölli, “Basic Radiobiology,” in *Radiation Oncology Physics: A Handbook for Teachers and Students*, E. B. Podgorsak, Ed. Vienna: International Atomic Energy Agency, 2005.

[6] B. M. C. Negritto, P. College, and N. Education, “Repairing Double - Strand DNA Breaks Why Is It So Important to Understand the Proteins Involved in the DNA Repair,” vol. 3, no. 2010, pp. 1–6, 2015.

[7] S. Elmore, “Apoptosis: a review of programmed cell death.,” *Toxicol. Pathol.*, vol. 35, no. 4, pp. 495–516, Jun. 2007.

[8] C. H. Jones, “Radiobiology of normal tissues,” in *Handbook of Radiotherapy Physics: Theory and Practice*, P. Mayles, A. Nahum, and J.-C. Rosenwald, Eds. Boca Raton, FL: Taylor & Francis Group, 2007.

[9] M. Goitein, “Biology Matters,” in *Radioation Oncology: A Physicist’s-Eye*, 1st ed., Springer, 2008.

[10] A.-L. Grosu, L. D. Sprague, M. Molls, A.-L. Grosu, ; L D Sprague, and ; M Molls, “Definition of Target Volume and Organs at Risk. Biological Target Volume,” in *New Technologies in Radiation Oncology*, Berlin Heidelberg, Germany: Springer, 2006, p. pp 167-177.

[11] M. Goitein, “Radiation in the treatment of cancer,” in *Radiation Oncology Physics: A Handbook for Teachers and Students*, 1st ed., Springer, 2008.

[12] B. (Paris) Desjardins, L.; Lumbroso-Le Rouic, L.; Levy-Gabriel, C.; Cassoux, N.; Dendale, R.; Mazal, A.; Delacroix, S.; Sastre, X.; Plancher, C.; Asselain, “Treatment of Uveal Melanoma by Accelerated Proton Beam,” in *Current concepts in uveal melanoma*, 1st ed., M. J. Jager, L. Desjardins, T. Kivelä, and B. E. Damato, Eds. Basel: KAGER, 2012.

[13] C. H. Jones, “Proton beams in radiotherapy,” in *Handbook of Radiotherapy Physics: Theory and Practice*, P. Mayles, A. Nahum, and J.-C. Rosenwald, Eds. Boca Raton, FL:

Taylor & Francis Group, 2007.

[14] M. Zehetmayer, “Stereotactic Photon Beam Irradiation of Uveal Melanoma,” in *Current concepts in uveal melanoma*, M. J. Jager, L. Desjardins, T. Kivelä, and B. E. Damato, Eds. Basel: KAGER, 2012.

[15] Z. Li, “Stereotactic radiosurgery and radiotherapy,” in *Technical Basis of Radiation Therapy*, 4th ed., S. Levitt, J. Purdy, and C. Perez et al., Eds. Berlin Heidelberg, Germany: Springer, 2006.

[16] N. Suntharalingam, E. B. Podgorsak, and H. Tölli, “Special procedures and techniques in radiotherapy,” in *Radiation Oncology Physics: A Handbook for Teachers and Students*, E. B. Podgorsak, Ed. Vienna: International Atomic Energy Agency, 2005.

[17] K. Dieckmann, D. Georg, M. Zehetmayer, J. Bogner, M. Georgopoulos, and R. Pötter, “LINAC based stereotactic radiotherapy of uveal melanoma: 4 years clinical experience,” *Radiother. Oncol.*, vol. 67, no. 2, pp. 199–206, May 2003.

[18] D. Georg, K. Dieckmann, J. Bogner, M. Zehetmayer, and R. Ptter, “Impact of a micromultileaf collimator on stereotactic radiotherapy of uveal melanoma,” *Int. J. Radiat. Oncol.*, vol. 55, no. 4, pp. 881–891, Mar. 2003.

[19] N. Suntharalingam, E. B. Podgorsak, and H. Tölli, “Brachytherapy: Physical and clinical aspects,” in *Radiation Oncology Physics: A Handbook for Teachers and Students*, E. . Podgorsak, Ed. Vienna: International Atomic Energy Agency, 2005.

[20] R. Pötter and E. Van Limbergen, “Uveal Melanoma,” in *The GEC ESTRO Handbook of Brachytherapy*, 1st ed., A. Gerbaulet, R. Pötter, J.-J. Mazeron, H. Meertens, and E. Van Limbergen, Eds. ESTRO, 2002.

[21] M. A. Astrahan, P. T. Finger, and D. S. Followill, “Dosimetry of 125 I and 103 Pd COMS eye plaques for intraocular tumors : Report of Task Group 129 by the AAPM and ABS,” *Med. Phys.*, vol. 39, no. 10, pp. 6161–6184, 2012.

[22] V. P. Papastefanou and V. M. L. Cohen, “Uveal melanoma.,” *J. Skin Cancer*, vol. 2011, no. 573974, 2011.

[23] E. R. Simpson *et al.*, “The American Brachytherapy Society consensus guidelines for plaque brachytherapy of uveal melanoma and retinoblastoma,” *Brachytherapy*, vol. 13, no. 1, pp. 1–14, 2014.

[24] S. M. Jaywant, E. K. Osei, and S. Ladak, “Stereotactic radiotherapy in the treatment of ocular melanoma: a noninvasive eye fixation aid and tracking system.,” *J. Appl. Clin. Med. Phys.*, vol. 4, no. 2, pp. 156–61, 2003.

[25] S. Akbaba *et al.*, “Linear accelerator-based stereotactic fractionated photon radiotherapy as an eye-conserving treatment for uveal melanoma.”

[26] J. Pe’er, “Ruthenium-106 Brachytherapy,” in *Current concepts in uveal melanoma*, 1st ed., M. J. Jager, L. Desjardins, T. Kivelä, and B. E. Damato, Eds. Basel: KAGER, 2012.

[27] G. Heilemann, “106Ru eye plaque brachytherapy – Benchmarking and evaluation of a

novel 3D treatment planning system for uveal melanoma Doctoral thesis at the Medical University of Vienna," Medical University of Vienna, 2017.

[28] D. Baltas, L. Sakelliou, and N. Zamboglou, "Brachytherapy Radionuclides and Their Properties," in *The Physics of Modern Brachytherapy for Oncology*, 1st ed., Boca Raton, FL: Taylor & Francis Group, 2007.

[29] G. Heilemann, N. Nesvacil, M. Blaickner, N. Kostiukhina, and D. Georg, "Multidimensional dosimetry of ^{106}Ru eye plaques using EBT3 films and its impact on treatment planning," *Med. Phys.*, vol. 42, no. 10, pp. 5798–5808, 2015.

[30] L. Mostafa, K. Rachid, and S. M. Ahmed, "Comparison between beta radiation dose distribution due to LDR and HDR ocular brachytherapy applicators using GATE Monte Carlo platform," *Phys. Medica*, vol. 32, no. 8, pp. 1007–1018, Aug. 2016.

[31] C. H. Jones, "Calibration and quality assurance of brachytherapy sources," in *Handbook of Radiotherapy Physics: Theory and Practice*, P. Mayles, A. Nahum, and J.-C. Rosenwald, Eds. Boca Raton, FL: Taylor & Francis Group, 2007.

[32] Z. Li, "Physics and Clinical Aspects of Brachytherapy," in *Technical Basis of Radiation Therapy*, 4th ed., S. H. Levitt, J. A. Purdy, C. A. Perez, and S. Vijayakumar, Eds. Berlin Heidelberg, Germany: Springer, 2006.

[33] "Assembling a COMS Plaque." [Online]. Available: https://www.eyephysics.com/PS/PS5/UserGuide/AssembleCOMS.html#insert. [Accessed: 03-May-2018].

[34] G. Heilemann *et al.*, "Treatment plan optimization and robustness of 106Ru eye plaque brachytherapy using a novel software tool," *Radiother. Oncol.*, vol. 123, no. 1, pp. 119–124, 2017.

[35] I. Buzatu, "A 3D Monte Carlo study of 125I COMS eye plaques for brachytherapy," Fachhochschule Technikum Wien, 2017.

[36] P. Braun, "Implementing dose lookup tables for 125 I COMS plaques into a novel treatment planning system for brachytherapy of uveal melanoma," Technical Universitiy of Vienna, 2018.

[37] Eckert & Ziegler BEBIG, "I-125 Ophthalmic Seeds," vol. 125, 2012.

[38] C. Groenewald, L. Konstantinidis, and B. Damato, "Effects of radiotherapy on uveal melanomas and adjacent tissues.," *Eye (Lond).*, vol. 27, no. 2, pp. 163–71, Feb. 2013.

[39] G. Heilemann *et al.*, "Retina dose as a predictor for visual acuity loss in 106Ru eye plaque brachytherapy of uveal melanomas," *Radiother. Oncol.*, vol. 127, no. 3, pp. 379–384, Jun. 2018.

Attachment

A. Tumor Coverage

The following tables summarize the absolute and relative $D_{98\%}$ dose values in Gray from the above mentioned simulations. The relative dose values were calculated in relation to a reference dose limit of 85 Gy. The tumor apex height varies from 3 to 8 mm in 0.5 mm steps and the tumor basal diameter from 5 to 20 mm in 1 mm steps. The tumor was placed in the central position with a distance of 11 mm to the optic nerve and the macula. Apart from the neutral plaque position the whole simulations were repeated for a plaque displacement of 1 and 2 mm.

Table 14: $D_{98\%}$ values in Gray of all the different tumor configurations of Plaque1 for the neutral position (0 mm displacement).

Plaque1												
apex height [mm]		**3**	**3.5**	**4**	**4.5**	**5**	**5.5**	**6**	**6.5**	**7**	**7.5**	**8**
tumor diameter [mm]	**5**	88.6	90.0	91.4	92.6	92.7	92.5	94.3	94.9	95.8	96.2	96.3
	6	88.5	89.8	91.1	92.4	92.7	92.5	94.1	94.7	95.5	95.8	96.2
	7	88.4	89.6	90.7	91.7	91.8	91.9	93.7	94.3	95.0	95.3	95.7
	8	88.0	89.2	90.1	90.7	91.3	91.6	93.3	93.8	94.0	94.5	95.3
	9	87.7	88.7	89.6	90.1	90.9	91.3	92.8	92.9	93.5	94.1	94.7
	10	87.0	87.8	88.5	89.3	90.3	90.5	91.8	92.0	92.8	93.4	93.9
	11	85.9	86.7	87.6	88.5	89.3	89.6	90.9	91.1	92.0	92.4	93.1
	12	84.7	85.6	86.6	87.4	88.0	88.7	89.9	90.1	90.8	91.4	92.2
	13	82.6	83.9	85.0	86.0	86.7	87.3	88.4	88.8	89.6	90.2	90.9
	14	79.2	80.8	82.3	83.8	84.6	85.6	86.8	87.2	88.0	88.7	89.4
	15	76.6	76.4	78.4	80.4	81.8	83.0	84.4	85.2	86.3	86.9	87.7
	16	70.3	73.7	73.1	75.4	77.4	79.0	80.8	82.2	83.6	84.4	85.5
	17	63.9	67.9	70.9	69.4	71.8	73.9	76.1	78.0	79.8	81.1	82.5
	18	60.0	61.3	63.2	66.9	65.5	67.8	70.4	72.8	75.0	76.5	78.4
	19	49.0	55.2	56.6	59.7	62.9	61.4	64.2	66.4	69.0	71.0	73.3
	20	36.9	43.3	48.7	52.3	54.6	59.4	59.8	59.5	62.2	64.6	67.1

Table 15: $D_{98\%}$ values in Gray of all the different tumor configurations of Plaque1 for 1 mm displacement.

Plaque1												
apex height [mm]		**3**	**3.5**	**4**	**4.5**	**5**	**5.5**	**6**	**6.5**	**7**	**7.5**	**8**
tumor diameter [mm]	**5**	89.0	89.6	91.4	92.2	92.8	92.3	95.1	95.4	95.4	96.4	96.2
	6	88.6	89.2	90.8	91.3	92.5	92.1	94.9	95.1	94.9	96.1	96.0
	7	87.9	88.4	89.9	90.7	92.0	91.6	94.3	94.3	94.1	95.2	95.6
	8	86.8	87.4	89.0	89.8	91.3	91.1	93.5	93.1	93.4	94.7	94.9
	9	85.7	86.7	88.2	89.1	90.5	90.2	92.5	92.5	92.8	94.0	94.2
	10	84.4	85.6	86.8	87.8	89.1	89.2	91.6	91.5	91.7	93.0	93.2
	11	82.8	83.5	85.2	86.4	87.8	87.8	90.2	90.3	90.6	91.9	92.2
	12	79.6	81.1	83.1	84.6	85.8	86.3	88.7	88.8	89.2	90.6	90.9
	13	76.4	78.1	80.4	81.8	83.4	84.4	86.5	87.0	87.6	89.0	89.4
	14	71.9	74.0	76.3	78.2	80.4	81.5	83.8	84.8	85.6	87.0	87.6
	15	70.3	69.4	71.7	74.0	76.4	77.7	80.4	81.6	82.7	84.5	85.3
	16	64.9	67.1	66.3	68.8	71.4	73.2	76.3	77.7	79.2	81.2	82.4
	17	59.1	61.4	64.5	63.4	66.2	68.0	71.2	73.0	74.8	77.1	78.5
	18	56.3	55.4	58.5	61.6	61.2	62.9	65.8	67.9	69.9	72.4	74.1
	19	48.3	50.7	52.3	55.7	58.8	57.6	60.2	62.1	64.3	67.0	69.0
	20	40.2	73.8	46.5	49.5	51.8	54.7	56.5	56.5	58.5	61.1	63.2

Table 16: $D_{98\%}$ values in Gray of all the different tumor configurations of Plaque1 for 2 mm displacement.

Plaque1												
apex height [mm]		**3**	**3.5**	**4**	**4.5**	**5**	**5.5**	**6**	**6.5**	**7**	**7.5**	**8**
tumor diameter [mm]	**5**	87.3	87.7	90.5	90.7	911.6	91.6	92.8	93.8	94.2	95.4	96.6
	6	86.7	87.0	89.9	90.1	90.9	91.0	92.8	93.4	93.7	95.1	96.1
	7	85.4	85.8	88.6	89.0	89.6	90.2	92.0	92.7	92.8	94.2	95.1
	8	83.3	84.2	87.4	87.3	88.4	89.2	90.9	91.5	91.7	93.2	94.1
	9	81.9	82.9	85.6	85.9	86.9	87.9	89.4	90.1	90.8	92.2	93.3
	10	79.0	79.9	82.9	84.1	85.2	86.0	87.7	88.8	89.2	90.6	91.8
	11	76.2	77.4	80.6	81.5	82.6	83.7	85.7	86.7	87.4	89.1	90.2
	12	72.0	73.6	76.8	78.3	79.8	81.4	83.3	84.5	85.3	87.2	88.3
	13	67.8	69.6	73.0	74.6	76.3	77.9	80.0	81.8	83.0	84.7	86.2
	14	63.2	65.0	68.3	70.1	72.4	74.3	76.7	78.5	79.8	81.9	83.7
	15	63.2	60.2	63.3	65.3	67.7	69.7	72.2	74.4	76.2	78.4	80.3
	16	56.2	58.0	58.5	60.5	63.0	65.1	67.7	70.1	72.0	74.5	76.6
	17	51.1	52.9	56.6	55.8	57.9	60.1	62.7	65.2	67.4	70.0	72.3
	18	48.8	47.9	51.6	54.2	53.5	55.3	57.9	60.4	62.+	65.4	67.8
	19	43.4	44.2	46.7	49.3	51.5	50.7	52.8	55.4	57.6	60.3	62.8
	20	37.8	40.3	42.7	43.9	45.5	48.4	50.1	50.7	52.4	55.0	57.5

Table 17: $D_{98\%}$ values in Gray of all the different tumor configurations of Plaque2 for the neutral position (0 mm displacement).

Plaque2												
apex height [mm]		**3**	**3.5**	**4**	**4.5**	**5**	**5.5**	**6**	**6.5**	**7**	**7.5**	**8**
tumor diameter [mm]	**5**	89.0	90.5	92.3	93.4	93.7	93.2	95.1	95.8	96.9	96.9	97.2
	6	88.7	90.1	91.7	92.8	93.5	93.2	94.9	95.5	96.4	96.4	97.0
	7	88.3	89.6	90.7	91.7	92.4	92.4	94.3	94.8	95.7	95.8	96.3
	8	87.4	88.5	89.6	90.8	91.6	91.8	93.4	94.0	94.6	95.0	95.7
	9	86.1	87.4	88.8	89.8	90.7	91.0	92.5	93.0	93.9	94.4	94.9
	10	84.2	85.7	87.2	88.3	89.3	89.6	91.2	91.8	92.8	93.1	93.8
	11	81.0	83.2	84.9	86.6	87.7	88.2	89.7	90.4	91.5	91.9	92.7
	12	77.1	79.6	82.1	84.3	85.6	86.4	88.0	88.8	89.9	90.4	91.3
	13	71.9	75.0	77.9	80.6	82.5	83.7	85.7	86.8	88.0	88.7	89.6
	14	65.9	69.3	72.8	76.1	78.4	79.9	82.4	84.1	85.7	86.6	87.6
	15	64.0	63.7	67.1	70.6	73.3	75.5	78.3	80.4	82.6	83.9	85.2
	16	57.1	61.0	61.0	64.3	67.6	70.2	73.3	75.7	78.4	80.1	81.9
	17	50.2	55.2	59.3	58.5	61.6	64.3	67.6	70.4	73.5	75.6	77.7
	18	46.9	49.2	52.2	56.2	55.4	58.2	61.6	64.7	67.9	70.3	72.8
	19	38.1	43.9	46.2	49.8	53.4	52.4	55.8	58.8	61.9	64.5	67.2
	20	29.2	35.0	39.7	43.4	46.1	50.8	52.2	52.5	55.5	58.3	61.1

Table 18: $D_{98\%}$ values in Gray of all the different tumor configurations of Plaque2 for 1 mm displacement.

Plaque2												
apex height [mm]		**3**	**3.5**	**4**	**4.5**	**5**	**5.5**	**6**	**6.5**	**7**	**7.5**	**8**
tumor diameter [mm]	**5**	88.9	89.6	91.5	92.1	93.4	93.9	95.9	96.3	96.3	96.9	97.7
	6	88.0	88.7	90.4	91.5	92.8	93.6	95.4	95.9	95.9	96.5	97.3
	7	86.1	87.3	89.4	90.6	91.9	92.6	94.4	94.8	94.9	95.5	96.8
	8	84.3	85.7	87.8	89.2	90.4	91.4	93.1	93.6	94.1.	94.8	95.8
	9	81.8	83.7	86.0	87.5	89.1	90.2	92.0	92.6	93.0	93.6	94.8
	10	78.4	80.8	83.3	85.2	87.0	88.3	90.3	91.0	91.5	92.3	93.6
	11	74.4	76.9	79.9	82.3	84.4	86.1	88.1	89.1	90.0	90.8	92.1
	12	69.4	72.4	75.6	78.6	81.2	83.2	85.6	86.9	87.9	89.0	90.5
	13	64.4	67.4	71.1	74.3	77.0	79.5	82.2	83.9	85.4	86.6	88.4
	14	59.2	62.3	65.9	69.1	72.3	75.2	78.2	80.3	82.2	83.9	85.8
	15	57.4	57.4	60.4	63.8	67.2	70.2	73.5	75.9	78.2	80.3	82.7
	16	52.3	55.3	55.3	58.3	61.7	64.9	68.4	71.1	73.7	76.0	78.7
	17	47.0	50.1	53.5	53.2	56.6	59.6	63.1	65.9	68.6	71.2	74.1
	18	44.6	44.6	48.1	51.8	52.0	54.7	57.8	60.6	63.5	66.2	69.2
	19	38.1	40.7	42.9	46.6	49.9	50.1	52.8	55.3	58.0	60.8	63.9
	20	31.7	35.2	38.1	41.3	44.0	47.8	49.8	50.3	52.7	55.2	58.3

Table 19: $D_{98\%}$ values in Gray of all the different tumor configurations of Plaque2 for 2 mm displacement.

Plaque2												
apex height [mm]		**3**	**3.5**	**4**	**4.5**	**5**	**5.5**	**6**	**6.5**	**7**	**7.5**	**8**
tumor diameter [mm]	**5**	86.5	86.9	90.2	91.1	91.8	92.2	93.1	94.4	95.3	96.6	97.2
	6	84.8	85.0	88.9	89.5	90.7	91.4	92.3	93.8	94.6	96.0	96.4
	7	81.8	82.9	86.8	88.0	88.9	90.0	91.1	92.7	93.3	94.7	95.1
	8	78.6	80.2	84.3	85.3	86.8	88.2	89.2	90.9	91.8	93.5	94.1
	9	75.3	77.0	80.9	82.7	84.5	86.1	87.3	89.1	90.5	92.1	92.7
	10	70.6	72.6	77.0	79.5	81.4	83.0	84.7	86.9	88.1	90.0	90.9
	11	66.0	68.3	72.9	75.2	77.6	79.6	81.8	84.0	85.7	87.8	88.8
	12	60.8	63.4	67.9	70.7	73.5	76.0	78.1	80.8	82.9	85.4	86.3
	13	56.0	58.6	63.0	65.9	68.8	71.5	74.0	77.1	79.4	82.0	83.6
	14	51.5	53.9	58.0	60.9	64.1	67.0	69.7	72.8	75.6	78.3	80.2
	15	49.9	49.3	52.9	55.8	59.0	62.0	64.8	68.2	71.1	74.2	76.2
	16	45.3	47.4	48.6	51.2	54.4	57.3	60.1	63.4	66.4	69.6	71.9
	17	40.9	43.0	47.0	47.1	49.9	52.7	55.3	58.6	61.6	64.8	67.3
	18	38.9	38.9	42.9	45.8	46.0	48.3	50.9	53.9	56.9	60.1	62.6
	19	34.7	36.0	38.7	41.8	44.4	44.2	46.4	49.4	52.3	55.3	57.8
	20	30.2	32.7	35.5	37.3	39.4	42.6	44.2	45.2	47.6	50.4	52.9

Table 20: Relative $D_{98\%}$ values compared to 85 Gy of all the different tumor configurations of Plaque1 for the neutral position (0 mm displacement).

Plaque1												
apex height [mm]		**3**	**3.5**	**4**	**4.5**	**5**	**5.5**	**6**	**6.5**	**7**	**7.5**	**8**
tumor diameter [mm]	**5**	104%	106%	108%	109%	109%	109%	111%	112%	113%	113%	113%
	6	104%	106%	107%	109%	109%	109%	111%	111%	112%	113%	113%
	7	104%	105%	107%	108%	108%	108%	110%	111%	112%	112%	113%
	8	104%	105%	106%	107%	107%	108%	110%	110%	111%	111%	112%
	9	103%	104%	105%	106%	107%	107%	109%	109%	110%	111%	111%
	10	102%	103%	104%	105%	106%	106%	108%	108%	109%	110%	110%
	11	101%	102%	103%	104%	105%	105%	107%	107%	108%	109%	109%
	12	100%	101%	102%	103%	104%	104%	106%	106%	107%	107%	108%
	13	97%	99%	100%	101%	102%	103%	104%	104%	105%	106%	107%
	14	93%	95%	97%	99%	100%	101%	102%	103%	104%	104%	105%
	15	90%	90%	92%	95%	96%	98%	99%	100%	102%	102%	103%
	16	83%	87%	86%	89%	91%	93%	95%	97%	98%	99%	101%
	17	75%	80%	83%	82%	84%	87%	90%	92%	94%	95%	97%
	18	71%	72%	74%	79%	77%	80%	83%	86%	88%	90%	92%
	19	58%	65%	67%	70%	74%	72%	75%	78%	81%	84%	86%
	20	43%	51%	57%	61%	64%	70%	70%	70%	73%	76%	79%

Table 21: Relative $D_{98\%}$ values compared to 85 Gy of all the different tumor configurations of Plaque1 for 1 mm displacement.

Plaque1												
apex height [mm]		**3**	**3.5**	**4**	**4.5**	**5**	**5.5**	**6**	**6.5**	**7**	**7.5**	**8**
tumor diameter [mm]	**5**	105%	105%	107%	108%	109%	109%	112%	112%	112%	113%	113%
	6	104%	105%	107%	107%	109%	108%	112%	112%	112%	113%	113%
	7	103%	104%	106%	107%	108%	108%	111%	111%	111%	112%	112%
	8	102%	103%	105%	106%	107%	107%	110%	110%	110%	111%	112%
	9	101%	102%	104%	105%	107%	106%	109%	109%	109%	111%	111%
	10	99%	101%	102%	103%	105%	105%	108%	108%	108%	109%	110%
	11	97%	98%	100%	102%	103%	103%	106%	106%	107%	108%	108%
	12	94%	95%	98%	100%	101%	102%	104%	105%	105%	107%	107%
	13	90%	92%	95%	96%	98%	99%	102%	102%	103%	105%	105%
	14	85%	87%	90%	92%	95%	96%	99%	100%	101%	102%	103%
	15	83%	82%	84%	87%	90%	91%	95%	96%	97%	99%	100%
	16	76%	79%	78%	81%	84%	86%	90%	91%	93%	96%	97%
	17	69%	72%	76%	75%	78%	80%	84%	86%	88%	91%	92%
	18	66%	65%	69%	73%	72%	74%	77%	80%	82%	85%	87%
	19	57%	60%	62%	65%	69%	68%	71%	73%	76%	79%	81%
	20	47%	52%	55%	58%	61%	64%	67%	67%	69%	72%	74%

Table 22: Relative $D_{98\%}$ values compared to 85 Gy of all the different tumor configurations of Plaque1 for 2 mm displacement.

Plaque1												
apex height [mm]		**3**	**3.5**	**4**	**4.5**	**5**	**5.5**	**6**	**6.5**	**7**	**7.5**	**8**
tumor diameter [mm]	**5**	103%	103%	106%	107%	108%	108%	109%	110%	111%	112%	114%
	6	102%	102%	106%	106%	107%	107%	109%	110&	110%	112%	113%
	7	100%	101%	104%	105%	105%	106%	108%	109%	109%	111%	112%
	8	98%	99%	103%	103%	104%	105%	107%	108%	108%	110%	111%
	9	96%	98%	101%	101%	102%	103%	105%	106%	107%	108%	110%
	10	93%	94%	98%	99%	100%	101%	103%	104%	105%	107%	108%
	11	90%	91%	95%	96%	97%	98%	101%	102%	103%	105%	106%
	12	85%	87%	90%	92%	94%	96%	98%	99%	100%	103%	104%
	13	80%	82%	86%	88%	90%	92%	94%	96%	98%	100%	101%
	14	74%	76%	80%	83%	85%	87%	90%	92%	94%	96%	98%
	15	74%	71%	74%	77%	80%	82%	85%	88%	90%	92%	94%
	16	66%	68%	69%	71%	74%	77%	80%	82%	85%	88%	90%
	17	60%	62%	67%	66%	68%	71%	74%	77%	79%	82%	85%
	18	57%	56%	61%	64%	63%	65%	68%	71%	74%	77%	80%
	19	51%	52%	55%	58%	61%	60%	62%	65%	68%	71%	74%
	20	44%	47%	50%	52%	54%	57%	59%	60%	62%	65%	68%

Table 23: Relative $D_{98\%}$ values compared to 85 Gy of all the different tumor configurations of Plaque2 for the neutral position (0 mm displacement).

Plaque2												
apex height [mm]		**3**	**3.5**	**4**	**4.5**	**5**	**5.5**	**6**	**6.5**	**7**	**7.5**	**8**
tumor diameter [mm]	**5**	105%	106%	109%	110%	110%	110%	112%	113%	114%	114%	114%
	6	104%	106%	108%	109%	110%	110%	112%	112%	113%	113%	114%
	7	104%	105%	107%	108%	109%	109%	111%	112%	113%	113%	113%
	8	103%	104%	105%	107%	108%	108%	110%	111%	111%	112%	113%
	9	101%	103%	104%	106%	107%	107%	109%	109%	110%	111%	112%
	10	99%	101%	103%	104%	105%	105%	107%	108%	109%	110%	110%
	11	95%	98%	100%	102%	103%	104%	106%	106%	108%	108%	109%
	12	91%	94%	97%	99%	101%	102%	103%	104%	106%	106%	107%
	13	85%	88%	92%	95%	97%	98%	101%	102%	104%	104%	105%
	14	78%	82%	86%	89%	92%	94%	97%	99%	101%	102%	103%
	15	75%	75%	79%	83%	86%	89%	92%	95%	97%	99%	100%
	16	67%	72%	72%	76%	80%	83%	86%	89%	92%	94%	96%
	17	59%	65%	70%	69%	72%	76%	80%	83%	86%	89%	91%
	18	55%	58%	61%	66%	65%	69%	72%	76%	80%	83%	86%
	19	45%	52%	54%	59%	63%	62%	66%	69%	73%	76%	79%
	20	34%	41%	47%	51%	54%	60%	61%	62%	65%	69%	72%

Table 24: Relative $D_{98\%}$ values compared to 85 Gy of all the different tumor configurations of Plaque2 for 1 mm displacement.

Plaque2												
apex height [mm]		**3**	**3.5**	**4**	**4.5**	**5**	**5.5**	**6**	**6.5**	**7**	**7.5**	**8**
tumor diameter [mm]	**5**	105%	105%	108%	108%	110%	110%	113%	113%	113%	114%	115%
	6	104%	104%	106%	108%	109%	110%	112%	113%	113%	113%	115%
	7	101%	103%	105%	107%	108%	109%	11%	112%	112%	112%	114%
	8	99%	101%	103%	105%	106%	108%	110%	110%	11%	111%	113%
	9	96%	99%	101%	103%	105%	106%	108%	109%	109%	110%	112%
	10	92%	95%	98%	100%	102%	104%	106%	107%	108%	109%	110%
	11	87%	90%	94%	97%	99%	101%	104%	105%	106%	107%	108%
	12	82%	85%	89%	92%	95%	98%	101%	102%	103%	105%	106%
	13	76%	79%	84%	87%	91%	94%	97%	99%	101%	102%	104%
	14	70%	73%	77%	81%	85%	88%	92%	94%	97%	99%	101%
	15	67%	67%	71%	75%	79%	83%	86%	89%	92%	94%	97%
	16	62%	65%	65%	69%	73%	76%	80%	84%	87&	89%	93%
	17	55%	59%	63%	63%	67%	70%	74%	77%	81%	84%	87%
	18	52%	52%	57%	61%	61%	64%	68%	71%	75%	78%	81%
	19	45%	48%	50%	55%	59%	59%	62%	65%	68%	72%	75%
	20	37%	41%	45%	49%	52%	56%	59%	59%	62%	65%	69%

Table 25: Relative $D_{98\%}$ values compared to 85 Gy of all the different tumor configurations of Plaque2 for 2 mm displacement.

Plaque2												
apex height [mm]		**3**	**3.5**	**4**	**4.5**	**5**	**5.5**	**6**	**6.5**	**7**	**7.5**	**8**
tumor diameter [mm]	**5**	102%	102%	106%	107%	108%	108%	109%	111%	112%	114%	114%
	6	100%	100%	105%	105%	107%	108%	109%	110%	111%	113%	113%
	7	96%	97%	102%	103%	105%	106%	107%	109%	110%	111%	112%
	8	92%	94%	99%	100%	102%	104%	105%	107%	108%	110%	111%
	9	89%	91%	95%	97%	99%	101%	103%	105%	106%	108%	109%
	10	83%	85%	91%	93%	96%	98%	100%	102%	104%	106%	107%
	11	78%	80%	86%	89%	91%	94%	96%	99%	101%	103%	104%
	12	71%	75%	80%	83%	86%	89%	92%	95%	97%	100%	102%
	13	66%	69%	74%	77%	81%	84%	87%	91%	93%	96%	98%
	14	61%	63%	68%	72%	75%	79%	82%	86%	89%	92%	94%
	15	59%	58%	62%	66%	69%	73%	76%	80%	84%	87%	90%
	16	53%	56%	57%	60%	64%	67%	71%	75%	78%	82%	85%
	17	48%	51%	55%	55%	59%	62%	65%	69%	72%	76%	79%
	18	46%	46%	50%	54%	54%	57%	60%	63%	67%	71%	74%
	19	41%	42%	46%	49%	52%	52%	55%	58%	61%	65%	68%
	20	36%	38%	42%	44%	46%	50%	52%	53%	56%	59%	62%

B. Organs at risk

The tables below show the simulated $D_{2\%}$ and D_{mean} values of the OARs such as the lens, the optic nerve, the macula, the retina and the ciliary body. Therefore, a tumor with a fixed basal diameter of 5 mm but three different apex heights (3, 5, 8 mm) was used and placed in three different positions (anterior, central and posterior). Additionally, to the neutral position of the plaque, its displacement from -2 to 2 mm along the retina was observed too. The values of the shifts are subdivided into two columns (min and max). The columns with the min heading include the negative displacement values and indicate a movement of the plaque away of the optic nerve. Conversely the values of the positive displacement are listed in the max columns and are representing a movement towards the optic nerve.

Table 26: $D_{2\%}$ and D_{mean} values in Gray of the lens, the optic nerve, the macula, the retina and the ciliary body for different plaque displacements (-2 to +2 mm) for the central position of the tumor.

			lens		optic nerv		macula		retina		ciliar body	
	error		$D_{2\%}$	D_{mean}	$D_{2\%}$	D_{mean}	$D_{2\%}$	D_{mean}	$D_{2\%}$	D_{mean}	$D_{2\%}$	D_{mean}
apex [mm]	0	3	39.1	25.6	28.9	22.0	26.3	21.4	164.2	40.8	63.3	28.3
		5	54.9	36.0	40.7	31.0	36.9	30.1	230.9	57.4	89.1	39.8
		8	88.1	57.8	65.2	49.7	59.2	48.3	370.1	92.1	142.8	63.7

			min		max		min		max		min		max		min		max		min		max	
	error		$D_{2\%}$	D_{mean}	$D_{2\%}$	D_{mean}	$D_{2\%}$	D_{mean}	$D_{2\%}$	D_{mean}	$D_{2\%}$	D_{mean}	$D_{2\%}$	D_{mean}	$D_{2\%}$	D_{mean}	$D_{2\%}$	D_{mean}	$D_{2\%}$	D_{mean}	$D_{2\%}$	D_{mean}
apex height [mm]	0.5	3	40.9	26.6	37.7	24.9	27.2	21.0	30.9	23.4	24.5	20.3	27.9	22.7	164.6	40.6	165.1	41.6	67.4	29.7	59.9	27.2
		5	57.3	37.2	52.8	35.0	38.2	29.4	43.4	32.8	34.4	28.4	39.1	31.9	230.9	56.9	231.5	58.3	94.5	41.6	84.0	38.2
		8	92.5	60.1	85.3	56.4	61.6	47.5	70.0	52.9	55.5	45.9	63.0	51.4	372.6	91.8	373.6	94.0	152.6	67.1	135.6	61.6
	1	3	42.7	27.6	36.4	24.3	25.8	20.0	33.3	24.8	23.4	19.4	30.4	24.3	165.8	40.3	165.7	43.0	72.2	31.1	56.4	26.3
		5	60.3	38.9	51.3	34.2	36.3	28.2	46.9	35.0	32.9	27.3	42.9	34.3	233.7	56.8	233.6	60.6	101.8	43.9	79.5	37.0
		8	95.8	61.8	81.6	54.4	57.8	44.9	74.6	55.6	52.3	43.4	68.2	54.5	371.5	90.3	371.3	96.4	161.8	69.7	126.3	58.8
	1.5	3	45.1	28.9	35.5	23.9	24.5	19.3	36.3	26.7	22.3	18.6	33.1	26.2	166.9	39.4	168.1	44.0	77.6	33.0	53.7	25.5
		5	63.1	40.4	49.7	33.4	34.2	27.0	50.7	37.4	31.2	26.0	46.3	36.6	233.4	55.2	235.1	61.6	108.6	46.1	75.1	35.7
		8	100.7	64.5	79.2	53.2	54.6	43.1	80.9	59.6	49.7	41.5	73.9	58.4	372.3	88.0	375.0	98.2	173.2	73.5	119.8	57.0
	2	3	47.3	30.0	34.3	23.3	23.4	18.5	39.2	28.5	21.2	17.9	35.7	28.2	163.6	39.0	169.1	44.8	82.6	34.5	50.7	24.7
		5	66.0	41.9	47.9	32.5	32.7	25.9	54.7	39.8	29.7	25.0	49.8	39.4	228.6	54.4	236.2	62.6	115.4	48.2	70.8	34.4
		8	105.5	67.0	76.5	52.0	52.2	41.3	87.5	63.7	47.4	39.9	79.6	62.9	365.3	87.0	377.4	100.1	184.4	77.1	113.1	55.0

Table 27: $D_{2\%}$ and D_{mean} values in Gray of the lens, the optic nerve, the macula, the retina and the ciliary body for different plaque displacements (-2 to +2 mm) for the anterior position of the tumor.

			lens		optic nerv		macula		retina		ciliar body	
	error		$D_{2\%}$	D_{mean}	$D_{2\%}$	D_{mean}	$D_{2\%}$	D_{mean}	$D_{2\%}$	D_{mean}	$D_{2\%}$	D_{mean}
apex [mm]	0	3	68.2	40.8	16.7	13.6	14.6	12.9	136.0	29.2	124.5	49.1
		5	95.9	57.4	23.4	19.1	20.5	18.1	191.3	41.0	175.0	69.1
		8	153.7	92.1	37.6	30.7	32.8	29.0	306.6	65.7	280.6	110.8

			min		max		min		max		min		max		min		max		min		max	
	error		$D_{2\%}$	D_{mean}	$D_{2\%}$	D_{mean}	$D_{2\%}$	D_{mean}	$D_{2\%}$	D_{mean}	$D_{2\%}$	D_{mean}	$D_{2\%}$	D_{mean}	$D_{2\%}$	D_{mean}	$D_{2\%}$	D_{mean}	$D_{2\%}$	D_{mean}	$D_{2\%}$	D_{mean}
apex height [mm]	0.5	3	71.4	42.6	65.4	39.4	16.1	13.1	17.4	14.2	14.1	12.5	15.3	13.4	130.3	28.1	141.8	30.2	129.6	51.2	120.7	47.5
		5	100.1	59.8	91.7	55.3	22.5	18.4	24.5	19.9	19.7	7.5	21.4	18.8	182.7	39.4	198.9	42.4	181.7	71.8	169.2	66.7
		8	161.5	96.4	148.0	89.2	36.4	29.8	39.5	32.1	31.8	28.3	34.5	30.3	294.9	63.5	321.0	68.4	293.2	115.9	273.0	107.6
	1	3	74.6	44.5	62.7	38.1	15.6	12.7	18.2	14.8	13.8	12.1	16.1	19.9	125.3	27.3	144.7	31.3	135.0	53.3	116.2	45.8
		5	105.2	62.7	88.3	53.7	22.0	18.0	25.7	20.9	19.4	17.1	22.7	19.6	176.6	38.5	204.0	44.1	190.3	75.1	163.8	64.6
		8	167.1	99.7	140.4	85.4	35.0	28.5	10.8	33.2	30.8	27.2	36.0	31.2	280.7	61.2	324.3	70.2	302.4	119.4	260.4	102.7
	1.5	3	78.5	46.8	60.7	37.1	15.2	12.4	19.4	15.7	13.4	11.9	17.0	14.7	123.8	26.7	152.1	33.3	139.6	55.7	112.4	44.5
		5	109.8	65.5	84.9	51.9	21.2	17.4	27.1	21.9	18.7	16.7	23.8	20.5	173.2	37.4	212.7	46.6	195.3	77.9	157.3	62.3
		8	175.1	104.5	135.4	82.8	33.8	27.8	43.2	34.9	29.8	26.6	38.0	32.7	276.2	59.7	339.3	74.3	311.5	124.3	250.8	99.3
	2	3	81.8	48.9	58.5	35.9	14.7	12.1	20.5	16.4	12.9	11.6	18.1	15.4	118.6	26.0	154.9	34.4	143.9	57.7	108.1	42.8
		5	114.3	68.2	81.7	50.1	20.5	16.9	28.6	22.9	18.0	16.2	25.2	21.5	165.7	36.4	216.3	48.1	201.0	80.6	151.0	59.8
		8	182.6	109.1	130.5	80.1	32.7	27.0	45.8	36.6	28.7	25.9	40.3	34.3	264.7	58.1	345.7	76.8	321.2	128.7	241.3	95.6

Table 28: $D_{2\%}$ and D_{mean} values in Gray of the lens, the optic nerve, the macula, the retina and the ciliary body for different plaque displacements (-2 to +2 mm) for the posterior position of the tumor.

			lens		optic nerv		macula		retina		ciliar body	
	error		$D_{2\%}$	D_{mean}	$D_{2\%}$	D_{mean}	$D_{2\%}$	D_{mean}	$D_{2\%}$	D_{mean}	$D_{2\%}$	D_{mean}
apex [mm]	0	3	27.6	19.8	59.7	40.7	66.5	47.3	176.2	53.4	35.1	19.8.
		5	38.0	27.3	82.1	56.0	91.5	65.0	242.2	73.5	48.2	27.2
		8	60.1	43.2	130.0	88.7	144.9	103.0	383.6	116.4	76.4	43.0

			min		max		min		max		min		max		min		max		min		max	
	error		$D_{2\%}$	D_{mean}	$D_{2\%}$	D_{mean}	$D_{2\%}$	D_{mean}	$D_{2\%}$	D_{mean}	$D_{2\%}$	D_{mean}	$D_{2\%}$	D_{mean}	$D_{2\%}$	D_{mean}	$D_{2\%}$	D_{mean}	$D_{2\%}$	D_{mean}	$D_{2\%}$	D_{mean}
apex height [mm]	0.5	3	29.2	20.8	34.0	23.4	56.2	38.7	37.6	27.9	60.5	44.4	38.9	30.4	180.6	55.2	180.	51.2	37.8	20.9	48.5	24.4
		5	39.6	28.3	46.2	31.8	76.3	52.5	51.0	37.9	82.1	60.2	52.8	41.3	245.1	74.9	244.3	69.5	51.3	28.4	65.8	33.1
		8	62.4	44.6	72.8	50.1	120.2	82.7	80.3	59.7	129.3	94.9	83.3	65.1	386.3	118.1	385.0	109.5	80.9	44.7	103.7	52.1
	1	3	30.7	21.7	34.6	23.8	52.1	36.4	38.3	28.4	55.5	41.4	39.7	31.0	184.0	55.0	183.3	52.1	40.4	21.9	49.4	24.8
		5	41.7	29.5	47.2	32.5	71.0	49.5	52.1	38.7	75.6	56.3	54.0	42.2	250.5	74.9	249.5	70.9	55.0	29.8	67.2	33.8
		8	64.8	45.9	73.3	50.4	110.3	76.9	80.9	60.1	117.4	87.5	83.8	65.6	289.0	116.4	387.6	110.2	85.4	46.4	104.4	52.5
	1.5	3	32.3	22.7	35.4	24.3	48.8	34.6	39.1	29.0	51.9	39.1	40.5	31.7	186.9	54.9	187.2	53.2	43.4	23.1	50.4	25.4
		5	43.9	30.8	48.0	33.1	66.2	47.0	53.0	39.4	70.5	53.0	55.0	43.0	253.7	74.5	254.1	72.2	58.9	31.4	68.4	34.4
		8	67.5	47.5	74.0	50.9	102.0	72.4	81.7	60.7	108.6	81.7	84.7	66.2	390.8	114.7	391.5	111.3	90.8	48.3	105.4	53.0
	2	3	34.4	24.0	36.5	25.1	46.4	33.4	40.4	30.0	48.6	37.1	41.8	32.7	192.5	56.7	193.4	55.0	47.2	24.6	52.1	26.2
		5	46.2	32.3	49.1	33.8	62.4	44.9	54.2	40.3	65.3	49.8	56.2	43.9	258.6	76.2	259.8	73.9	63.5	33.1	70.0	35.2
		8	70.3	49.1	74.6	51.4	94.8	68.3	82.4	61.2	99.3	75.7	85.4	66.8	393.1	115.8	394.9	112.3	96.5	50.3	106.4	53.5